A Review of Techniques for Measuring the Biot Coefficient and Other Effective Stress Parameters for Fluid-Saturated Rocks

Hossein A. Kasani[1]
Nuclear Waste Management Organization (NWMO),
Toronto, ON M4T 2S3, Canada
e-mail: hkasani@nwmo.ca

A. P. S. Selvadurai
Department of Civil Engineering and Applied Mechanics,
McGill University,
Montreal, QC H3A 0C3, Canada
e-mail: patrick.selvadurai@mcgill.ca

Predicting the behavior of a saturated rock with variations in pore fluid pressure during geo-energy production and storage, deep geological disposal of nuclear wastes, etc. with skeletal mechanical behavior in the linear elastic range is carried out using the isothermal theory of poroelasticity that incorporates Biot's effective stress principle. For conditions that are not within linear elasticity, other effective stress coefficients are used. Several experimental methods for determining Biot's and other effective stress coefficients have been documented in the literature. The objective of this study is to review the fundamentals of these techniques, their advantages and disadvantages, and to include several case studies. Current techniques for Biot's coefficient are based on different premises: jacketed and unjacketed bulk moduli or compressibility values; volume changes of the bulk and pore fluid from a drained triaxial test on a saturated sample; isotropic-isochoric compression tests on a saturated sample; matching volumetric strains for dry and saturated samples; estimation of the Biot coefficient from other poroelastic parameters; and approximation of the jacketed bulk modulus from ultrasonic wave velocities and/or unjacketed bulk modulus from the mineralogical compositions. Other effective stress coefficients are based on matching failure envelopes for dry and saturated samples and variations of rock properties (such as volumetric strain, permeability, and ultrasonic wave velocities) with respect to confining stress and pore pressure. This article discusses variations in Biot's and other effective stress coefficients produced using the different techniques and how factors such as pore geometry, test conditions, stress path, and test temperature affect the coefficients. [DOI: 10.1115/1.4055888]

Keywords: the Biot coefficient, effective stress coefficient, poroelasticity, jacketed test, unjacketed test

1 Introduction

The motivation for this study is derived from the pioneering papers by Biot [1] and Biot and Willis [2] that laid out the guiding principles of poroelasticity for an isotropic porous solid, which has been used across various disciplines for eight decades. Energy-related subsurface activities and other processes such as oil and gas exploitation [3–10], underground CO_2 sequestration [11,12], hydraulic fracturing [13,14], enhanced geothermal systems or EGS [15,16], underground compressed air energy storage or CAES [17,18], deep geological disposal of nuclear waste [19–22], underground wastewater disposal [23,24], longwall mining [25], wellbore stability [26,27], fault re-activation due to fluid pressure increase [28,29], water level changes in wells [30], tide effects on compressible aquifers [31], and glacial advance and retreat [32] contribute to perturbations in the geosphere in terms of changes to the total stresses, pore pressures, and the thermal regime. The impacts of these processes often result in coupled hydro-mechanical (HM) or thermo-hydro-mechanical (THM) phenomena where the responses of fluid-saturated rock masses need to be predicted [33,34]. Other field processes such as in situ seismic wave velocity measurements [35,36] also involve the response of a saturated rock. Similarly, interpretation of THM loading of a rock in laboratory conditions involves the behavior of the fluid-saturated rock [37–39]. The rock response, however, is dependent on how the external stresses are partitioned between the solid skeleton and the pore fluid. The partitioning for the linear elastic state can be estimated using Biot's theory of poroelasticity [1], where Biot expressed stresses as functions of strains, elastic properties, and fluid pressure or increment of the fluid volume per unit volume of the porous rock. The original definition of Biot's effective stress has been continually extended to account for nonlinear and inelastic behavior of the rock; therefore, succeeding studies used a general effective stress framework similar to that of Biot's where the pore pressure factor was called the effective stress coefficient (some referred to it as the effective pressure coefficient) for the stress regimes which fall outside Biot's linear poroelasticity.

This article reviews Biot's theory of three-dimensional consolidation [1] concerning the relationship between strain, stress, pore fluid pressure, and the pore fluid volume increment for a porous material at an equilibrium condition (no transient pore fluid pressure effects). Fundamentals of the theory of linear poroelasticity have been reviewed by many investigators [40,41]. The theory of poroelasticity has been extensively applied to geomaterials, for example, see Ref. [42] for a review of applications of this theory to various analytical problems in geomechanics, and Ref. [43] for a review of applications to shearing and failure of geomaterials. Biot [1] and Biot and Willis [2] introduced a scalar multiplier for the pore pressure term in the stress–strain-fluid pressure relationship, which is commonly known as the Biot coefficient α. An overview of the original derivations of the analytical relations for

[1]Corresponding author.

Manuscript received March 19, 2022; final manuscript received September 27, 2022; published online November 3, 2022. Assoc. Editor: Samantha H. Daly.

α by Biot [1] and Biot and Willis [2] is provided here, followed by the various experimental methods reported in the literature for determining the Biot coefficient. The paper continues with a review of other effective stress (or pressure) coefficients introduced by successive investigators for conditions that do not follow the linear poroelasticity. The advantages and disadvantages of each technique in conjunction with several case studies are explained. An abridged version of this review was recently published by the lead author [44]. It should be noted that measuring the effective stress coefficient of unsaturated rocks is beyond the scope of this article and can be found elsewhere [45–47]. The Biot coefficient for skeletal elastoplastic conditions also falls outside the scope of this review and the reader is referred to Ref. [48], for incorporating elastoplastic effects.

2 An Overview of Biot's Theory of Three-Dimensional Consolidation

2.1 Relationship Between Strain, Stress, Fluid Content, and Fluid Pressure for an Isotropic Elastic Porous Material. Biot [1] extended the classical elastic stress–strain relationship for an isotropic poroelastic material to include the pore pressure term (P). In Cartesian tensor notation, the constitutive relation for an isotropic material can be written as

$$\varepsilon_{ij} = \frac{\sigma_{ij}}{2G} - \left(\frac{1}{6G} - \frac{1}{9K}\right)\sigma_{kk}\delta_{ij} + \frac{P}{3H}\delta_{ij} \tag{1}$$

where σ_{ij} and ε_{ij} are the classical Cauchy stress and small strain tensor, respectively, in an infinitesimal cuboidal element of the porous material. As is common in solid mechanics, stress and strain are assumed positive in extension, P is assumed to be positive when it results in extension, G and K are the shear and bulk modulus of the drained elastic solid, respectively, δ_{ij} is the Kronecker delta, and H is a new physical constant.

Biot [1] introduced a new variable as the variation of fluid content (ξ) which is equal to the increment of fluid volume per unit volume of the porous medium: a positive ξ corresponds to a gain of fluid by the porous material. Since the developments focus on ideal fluids, the shear stresses do not affect the fluid content, and the effect of normal stresses on fluid content is assumed to be isotropic. Therefore, the fluid content-stress-fluid pressure may be written as Eq. (2) where H' and R are two physical constants

$$\xi = \frac{\sigma_{kk}}{3H'} + \frac{P}{R} \tag{2}$$

In the case of an isotropic stress state, the potential energy increment per unit volume of the saturated porous material is given by

$$dW = \frac{1}{2}(\sigma_{ij}\, d\varepsilon_{ij} + P\, d\xi) = \frac{1}{2}(\varepsilon_{ij}\, d\sigma_{ij} + \xi\, dP) \tag{3}$$

Assuming that the work done to bring the material from its initial state to the final condition of strain and fluid content is path-independent implies that

$$\frac{\partial \varepsilon_{ij}}{\partial P} = \frac{\partial \xi}{\partial \sigma_{ij}} \tag{4}$$

Equation (4) combined with Eqs. (1) and (2) leads to $H = H'$.

Equations (1) and (2) are the fundamental relations for a linear isotropic porous material under equilibrium conditions with respect to strain and fluid content, and are dependent on four physical constants G, K, H, and R. Rewriting Eqs. (1) and (2) with respect to stresses, Eq. (5) is obtained

$$\sigma_{ij} = 2G\varepsilon_{ij} + \lambda\, \varepsilon_{kk}\, \delta_{ij} - \alpha P \delta_{ij} \tag{5}$$

where λ is Lamé's parameter under drained conditions (i.e., constant pore pressure) defined in Eq. (6) and α is a constant defined in Eq. (7)

$$\lambda = \frac{E\nu}{(1+\nu)(1-2\nu)} \tag{6}$$

$$\alpha = \frac{K}{H} \tag{7}$$

where E is Young's modulus and ν is Poisson's ratio under drained condition. Substituting Eq. (5) in Eq. (2), the variation in fluid content can be expressed as

$$\xi = \alpha\, \varepsilon_{kk} + \left(\frac{1}{R} - \frac{\alpha}{H}\right)P \tag{8}$$

A more complete presentation of the equations presented in this section can be found in texts on poroelasticity (e.g., Refs. [49] and [50]).

2.2 An Implied Effective Stress Relationship and Biot Effective Stress Coefficient for Isotropic Elastic Porous Material. The analytical development of Biot [1] as defined by Eq. (5) is an effective stress relation. The first two terms on the right side of Eq. (5) lead to the corresponding normal strain induced by the total stress and the third term is the pore pressure term multiplied by the pore pressure parameter, which is referred to as the Biot coefficient, see, e.g., Ref. [51]. Although Biot [1] and Biot and Willis [2] did not specifically refer to this as the effective stress coefficient, it is implied and used in the literature. The stress–strain-pore pressure relation of Eq. (5) (Eq. (2.11) in Biot [1]), is associated with an effective stress equation that is similar in nature to the effective stress equation introduced by Terzaghi [52]. As is commonly used in the literature, any equation that is a relationship between the total stress, the skeletal stress, the fluid pressure, and the relevant constitutive properties of the geomaterial is an effective stress equation. Biot's effective stress relationship assumes that the total isotropic confining stress (σ_{ij}), or total stress (as used by many authors in the literature), is the sum of the effective stress or σ'_{ij} (i.e., the stress carried by the porous skeleton), and the pore fluid pressure (P) multiplied by a constant, α, which is commonly referred to as the Biot coefficient or, in much of the literature, as the Biot–Willis coefficient [2], and defined by Eq. (9)

$$\sigma'_{ij} = \sigma_{ij} - \alpha P \delta_{ij} \tag{9}$$

Biot [1] applied his theory of three-dimensional consolidation to two specials test conditions, namely, jacketed and unjacketed compressibility tests. In the jacketed test, where there is no variation in pore pressure in Eq. (8), α measures the ratio of the fluid volume increment to the volume change of the elastic porous solid, that is

$$\alpha = \frac{\xi}{\varepsilon_{kk}} \tag{10}$$

Biot and Willis [2] considered the jacketed and unjacketed compressibility test conditions in Eqs. (1). In the jacketed test, an isotropic stress of $\sigma_{ij} = -\sigma\delta_{ij}$ is applied to the porous material, $P = 0$, and the shear stresses are zero. The volumetric strain and jacketed bulk modulus (K) of the porous material (inverse of jacketed compressibility) are related through

$$\varepsilon_{kk} = \frac{-\sigma}{K} \tag{11}$$

Hence for the jacketed compressibility test, Eq. (5) yields

$$-\sigma = 2G\left(\frac{-\sigma}{3K}\right) + \lambda\left(\frac{-\sigma}{K}\right) \tag{12}$$

In the unjacketed test, an isotropic (compressive) stress of $\sigma_{ij} = -\sigma\delta_{ij}$ is applied on the solid skeleton, the fluid pressure is equal to $P = \sigma$, and the shear stresses are zero. The volumetric strain and unjacketed bulk modulus (K_s) of the porous material (inverse of unjacketed compressibility) are related through

$$\varepsilon_{kk} = \frac{-\sigma}{K_s} \tag{13}$$

Substituting the results for the unjacketed compressibility test into Eq. (5), we can write

$$-\sigma = 2G\left(\frac{-\sigma}{3K_s}\right) + \lambda\left(\frac{-\sigma}{K_s}\right) - \alpha\sigma \tag{14}$$

Solving Eqs. (12) and (14) for α and eliminating σ, Biot and Willis [2] derived Eq. (15) which is usually referred to as the original definition of the Biot coefficient or the jacketed-unjacketed method

$$\alpha = 1 - \frac{K}{K_s} \tag{15}$$

In the literature, K_s is commonly referred to as the bulk modulus of the solid phase or grains. In the case of an ideal homogeneous rock composed of only one mineral (and no pore space), the unjacketed modulus or K_s is equal to the bulk modulus of the mineral or K_s'.

With low-porosity and low permeability rocks, there is an unacceptably long testing period required to reach equilibrium of the pore fluid pressure, which is a prerequisite for determining α. Furthermore, there are no assurances that the entire pore space is saturated with the pore fluid. This has posed a challenge to the rock mechanics community dealing with applications of poroelasticity [53,54]. Consequently, researchers proposed various methods to either directly determine the Biot coefficient or to approximately determine it through the consideration of contributions to the two components of the bulk moduli encountered in Eq. (15). The developments were based on deriving new analytical results from the original definition of Biot [1] and Biot and Willis [2] or the concept that the response of a fluid-saturated rock is dominated by the effective stress. The latter idea opened a new gateway to compare the responses of dry and saturated rock samples to estimate the effective stress, and hence, the Biot coefficient. The original definition of effective stress by Biot [1] and Biot and Willis [2] is constantly being extended to include nonlinear and inelastic skeletal properties, therefore, this review regards α as the Biot effective stress coefficient relevant to isotropic linear poroelasticity only. In much of the literature, the Biot [1] and Biot–Willis [2] solutions are referred to as the "conventional" or "direct" techniques. However, other researchers have referred to the physical experiments therein and called the technique the "jacketed-unjacketed" test method. Several published articles used the terms "direct" versus "indirect" methods. While all these terms (jacketed–unjacketed, direct, indirect, etc.) are used throughout this review; the intention is to prevent any bias in choosing only one of these descriptors for the methods discussed herein. In a general sense, any techniques that were established based on the analytical definition for α following the original suggestion by Biot [1] or Biot and Willis [2] are generally called direct methods. The estimation of α or its components using other methods are thus referred to as indirect methods (e.g., the method based on an estimation of the bulk or grain modulus).

2.3 Limits of the Biot Effective Stress Coefficient for an Isotropic Elastic Porous Geomaterial

2.3.1 Upper Limit. Triaxial experiments under isotropic stress conditions are used to reliably measure K_s in soil-like materials and weak porous rocks without excessive time demands to attain equilibrium of the applied stresses. If $K \ll K_s$ (e.g., isotropic saturated soils), α approaches unity. Biot and Willis [2] examined the limits of the coefficient α. They discussed that α for an elastic isotropic material cannot be greater than unity. This is because K in Eq. (15) is positive and cannot be zero, and K_s is also positive. Similarly, given that the fluid volume change in a jacketed test cannot exceed the total volume change, α in Eq. (10) must satisfy the condition of $0 \leq \alpha \leq 1$.

If $\alpha = 1$, Biot's effective stress reduces to Terzaghi [52] effective stress (Eq. (16)), where σ_s' is the simple effective stress

$$\sigma_s' = \sigma - P \tag{16}$$

Terzaghi's effective stress equation is very simple in form and widely used in soil mechanics; however, the simple relationship does not contain any influence of the constitutive properties of the porous material and the solid phase that will guide a user toward making an appropriate simplification [55].

Measuring the unjacketed bulk modulus in low-porosity rocks poses considerable challenges due to the time required for (i) the pore fluid to saturate the pore space and (ii) achieving equilibrium under the applied stresses. Estimation of K_s for this class of materials can also introduce errors in the calculation of α. Nevertheless, the bulk modulus in low-porosity rocks approaches the bulk modulus of the solids; hence, according to Eq. (15) α becomes much smaller than that for soils and approaches its lower limit.

2.3.2 Lower Limit. Biot and Willis [2] rewrote Eq. (5) by replacing the pore pressure term with the variation in fluid content term (Eq. (17)), where Q is a new physical constant

$$\sigma_{ij} = 2G\varepsilon_{ij} + \lambda\,\varepsilon_{kk}\,\delta_{ij} + Q\xi\delta_{ij} \tag{17}$$

The skeletal shear stresses are not influenced by pore pressure or variations in the fluid content. Pore pressure is now defined by Eq. (18) where R_1 is a new physical constant

$$P = Q\,\varepsilon_{kk} + R_1\,\xi \tag{18}$$

To define the lower limit of α, Biot and Willis [2] once again considered the jacketed and unjacketed compressibility tests in Eq. (17) in conjunction with the pore pressure relation of Eq. (18).

In the jacketed test, an isotropic stress of $\sigma_{ij} = -\sigma\,\delta_{ij}$ is applied on the solid skeleton, $P = 0$, and shear stresses are zero. The normal strain and volumetric strain of the porous solid can be determined from Eq. (11) by knowing the jacketed bulk modulus. Substituting this information in Eq. (17) yields

$$-\sigma = 2G\left(\frac{-\sigma}{3K}\right) + \lambda\left(\frac{-\sigma}{K}\right) + Q\xi \tag{19}$$

From $P = 0$ condition

$$0 = Q\left(\frac{-\sigma}{K}\right) + R_1\xi \tag{20}$$

Eliminating σ and ξ gives

$$K = \frac{2}{3}G + \lambda - \frac{Q^2}{R_1} \tag{21}$$

Here, for the unjacketed test, as is common in Soil Mechanics and poromechanics, an isotropic (compressive) stress of $\sigma_{ij} = -\sigma\delta_{ij}$ is partitioned between the portion taken by the fluid or $P = -\text{Ø}\sigma$ and the portion taken by the solid phase of the porous material which is equal to $\sigma_{ij} = -(1-\text{Ø})\sigma\delta_{ij}$. This approach helps bring the porosity (Ø) term into the discussion. The normal strain and volumetric strain of the porous solid can be determined from

Eq. (13) by knowing the unjacketed bulk modulus. Substituting this information in Eqs. (17) and (18) yields

$$-(1-\text{Ø})\sigma = 2G\left(\frac{-\sigma}{3K_s}\right) + \lambda\left(\frac{-\sigma}{K_s}\right) + Q\xi \tag{22}$$

$$-\text{Ø}\sigma = Q\left(\frac{-\sigma}{K_s}\right) + R_1\xi \tag{23}$$

Eliminating σ and ξ yields

$$1-\left(\frac{Q+R_1}{R_1}\right)\text{Ø} = \left(\frac{2}{3}G+\lambda-\frac{Q^2}{R_1}\right)\frac{1}{K_s} \tag{24}$$

Substituting Eq. (21) into Eq. (24) yields

$$\left(\frac{Q+R_1}{R_1}\right)\text{Ø} = 1-\frac{K}{K_s} \tag{25}$$

Comparing these results with Eq. (15), α can be defined as

$$\alpha = \left(\frac{Q+R_1}{R_1}\right)\text{Ø} \tag{26}$$

From Eq. (18), if a positive fluid pressure is applied to the porous material while at the same time the volumetric strain is held fixed, a positive fluid content increment must result; R_1 must therefore be positive. Alternatively, if the fluid pressure is held constant and a positive stress is applied, the volumetric strain must be positive while there is a net increase in the porosity. Thus, there is a negative fluid content increment, and Q must be positive. Since both R_1 and Q are positive, it can be concluded from Eq. (26) that α cannot be smaller than the porosity of the porous material.

The trivial lower limit for the Biot coefficient can also be approached by considering the basic definition for α given by Eq. (15). If the skeletal material is monomineralic and if the porosity tends to zero, then it is feasible to assume that $K \to K_s$, and in this case $\alpha \to 0$.

Alternative expressions for Eqs. (17) and (18) for undrained conditions, incorporating undrained elastic parameters and Skempton's pore pressure parameter B, can be found elsewhere, e.g., Cheng [33], Detournay and Cheng [49], and Rice and Cleary [56].

3 Fundamentals of the Direct and Indirect Techniques for Determining the Biot Coefficient

In this section, the original method for determining the Biot coefficient from Biot [1] and Biot and Willis [2] and other developments are discussed along with the advantages and disadvantages of each method. Several case studies for each technique from the literature are summarized to show the range of applicability of each method. In the remainder of this review, as is common in rock mechanics, compressive stress and strain are assumed to be positive.

3.1 Jacketed–Unjacketed Tests. The fundamentals of jacketed and unjacketed compressibility tests are provided in Sec. 2.2 and the common relationship between the bulk and solid moduli are shown by Eq. (15). Nur and Byerlee [57] later provided an alternative theoretical solution and independently proved that Eq. (15) is theoretically exact. The solution given in Ref. [57] is discussed here for completeness. Assuming that the solid skeleton is homogeneous, isotropic, and linear elastic over the range of the applied stresses and the pore spaces are fully interconnected, Ref. [57] calculated the elastic volumetric strain of a rock sample under an externally applied confining stress, σ, and an internally applied pore fluid pressure P. By superposition of the volumetric strains under only P and for the case where the medium is under an external confining stress of $\sigma - P$ (Fig. 1), Eq. (15) was achieved. This equation is traditionally used in poroelasticity and is also known as the original method for determining α. It is sometimes referred to as the method based on jacketed – unjacketed bulk moduli or compressibilities. Reference [57] also used the term effective stress for the relationship between stress, strain, and pore pressure proposed by Biot [1].

Nur and Byerlee [57] also experimentally demonstrated the validity of Eq. (15). They conducted several isotropic compression tests on saturated and dry samples of the Weber sandstone. Pretest porosity (Ø) of the sandstone was about 6%. Tap water was used as the pore fluid for the tests on the saturated samples. The results of the tests are presented in Fig. 2. The volumetric strain plotted against the total confining stress (Fig. 2(*a*)) shows a significant scatter. Plotting the data against $\sigma - P$ slightly improved the scatter (Fig. 2(*b*)); however, the scatter of the data was remarkably reduced when they were plotted against Biot's effective stress as defined by Eq. (9) and shown in Fig. 2(*c*).

According to Biot and Willis [2], use of Eq. (9) requires the measurement of the matrix and grain compressibility or bulk moduli. Generally, two triaxial isotropic compression tests are required to determine α; a test on a jacketed specimen (which is dry with no fluid saturation, or a drained test carried out on a saturated specimen provided sufficient time is allowed for the fluid pressure to equilibrate) to measure K (using Eq. (11)) and a test on an unjacketed specimen to determine K_s (using Eq. (13)).

In the jacketed test, an external confining stress is applied to the specimen and varied over a specified range while the pore pressure is maintained constant (drained condition). This test can also be conducted on a dry specimen. However, Biot and Willis [2] pointed out that the dry specimen may not exhibit the same properties as the saturated specimen; an example could be the case where the elastic properties are affected by capillary forces at the interface of the pore fluid and the solid grains.

In the unjacketed test, a pressure $\sigma = P$ is applied to the sample. The unjacketed test can also be carried out on a jacketed specimen provided that the increments of the pore and confining pressures are identical. Under the loading condition in an unjacketed test, any measured deformation is that of the solid phase. In an unjacketed test, the rock should either be highly permeable or a low strain rate should be used, which is crucial for draining the pore water in a practical experimental time frame.

If the porous skeleton is homogeneous and composed of only one mineral, then K_s is equal to the bulk modulus of the constituent mineral. If the porous skeleton is inhomogeneous and composed of several minerals (as occurs in most rocks), then K_s represents a weighted average of the bulk moduli of the constituent minerals [58,59]. Other approaches based on theories for effective properties for multiphasic elastic solids have also been used recently to provide estimates for the solid material compressibilities for the Cobourg limestone, Grimsel granite, and Lac du Bonnet granite [53,60,61], respectively.

The unjacketed bulk modulus is independent of the stress level in the elastic domain. For the low-porosity Westerly granite (porosity Ø $\sim 1\%$) and under $\sigma = 0 - 250$ MPa, Nur and Byerlee [57] measured $K_s = 45.5$ GPa (Fig. 3). Reference [62] also reported a constant $K_s = 41.2$ GPa from an unjacketed test on the Flechtinger sandstone (Ø = 9.1–10.8%) under stresses between 2 MPa and 55 MPa.

In contrast, some publications have reported a variable K_s. For example, Ref. [63] reported nonlinearity in an unjacketed test on the Castlegate sandstone; they deduced that K_s was between 52.28 GPa and 60.70 GPa as the confining stress increased from 22 MPa to 144 MPa. However, the justification for this odd behavior is not clear to the authors of this review. Reference [64] found that K_s of a Vosges sandstone increased from 28.1 GPa to 52.9 GPa as confining stress increased from 5 MPa to 25 MPa; they attributed this behavior to the possible closure of the

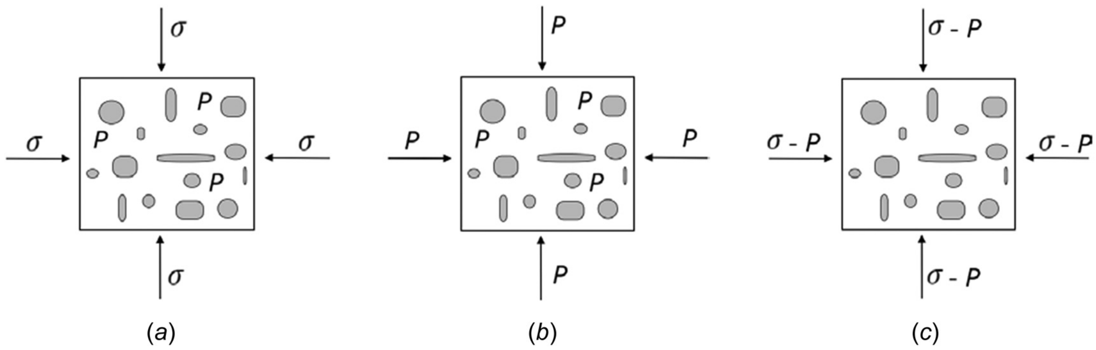

Fig. 1 The assumptions made by Nur and Byerlee [57] in independently deriving the analytical solution of the Biot and Willis [2] coefficient and calling it the effective stress coefficient, α: (*a*) elastic porous medium under the effect of σ and *P*, (*b*) elastic porous medium subjected to $\sigma = P$ (the unjacketed test), and (*c*) elastic porous medium under $\sigma - P$ (the jacketed test)

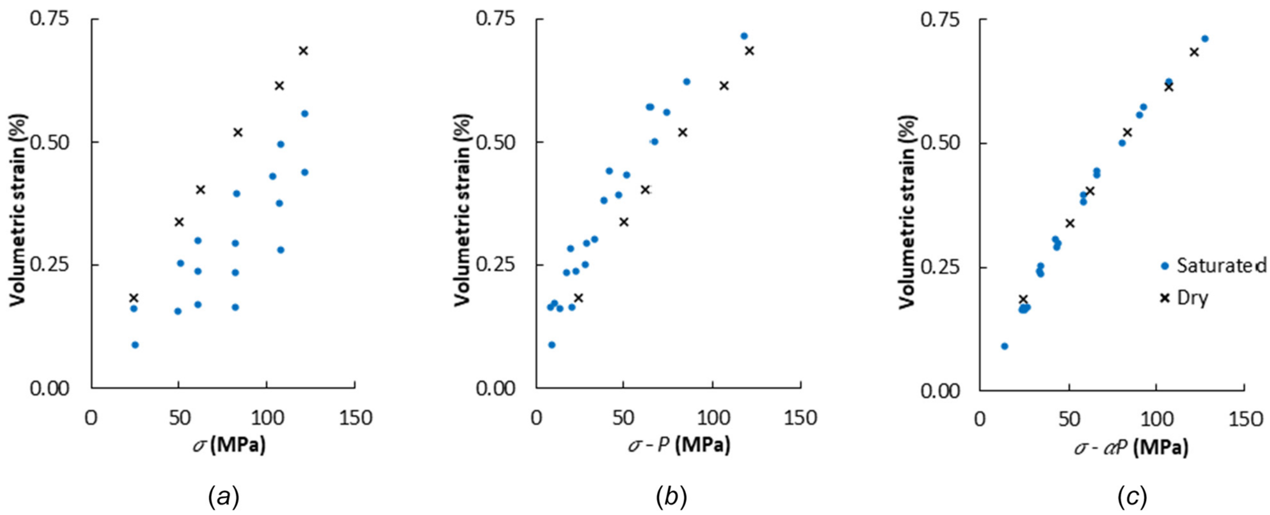

Fig. 2 Experimental validation of Eq. (15) on the Weber sandstone (Ø = 6%) from Ref. [57]: (*a*) volumetric strain versus total confining stress, (*b*) volumetric strain versus effective stress where $\alpha = 1$, and (*c*) volumetric strain versus effective stress using α as defined by Eq. (15)

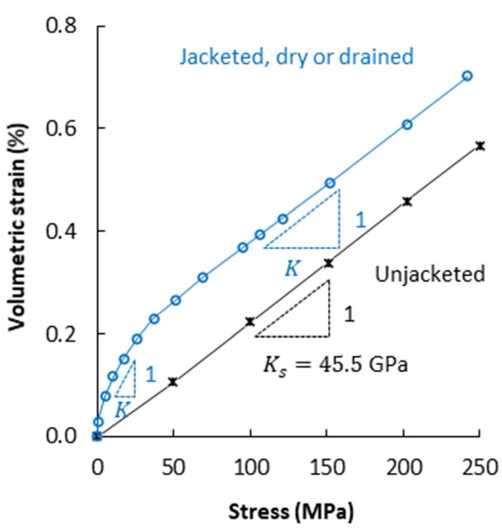

Fig. 3 Volumetric strains for the Westerly granite (Ø = 1%) in an unjacketed and a jacketed test [57] and the associated determinations of K_s and *K*. Note that *K* is dependent on the stress level; however, it approaches K_s when $\sigma > 100$ MPa.

microcracks as a result of the increased confining stress. However, the authors of this review cannot confirm their justification.

The bulk modulus of a porous rock (K) is dependent on the magnitude of the applied confining stress and pore pressure. As shown in Fig. 3, the bulk modulus of Westerly granite increased as σ increased; however, K approached K_s at about $\sigma = 100$ MPa, and was attributed by the authors [57] to possible pore closure. According to Ref. [64], the bulk modulus of the Berea sandstone remained constant at $\sigma > 30$ MPa; however, they did not provide any explanation for this behavior.

Table 1 summarizes several case studies on rocks where the Biot coefficient was measured using the jacketed-unjacketed testing technique. Cylindrical sample diameter and length are represented by symbols D and L, respectively. The table includes several sedimentary and crystalline rocks, such as the Westerly granite, Flechtinger sandstone, Berea sandstone, Castlegate sandstone, Indo-Chinese granodiorite, Callovo-Oxfordian claystone, Opalinus clay, Sorcy limestone, Eau Claire shale, Charcoal granite, and Lac du Bonnet granite, where values between 0.04 and 1.00 were reported for the Biot coefficients. Initial sample porosities before testing were between <0.5% and 28.4%. The table includes a wide range of confining stresses from 0 to 240 MPa. The pore fluids used were water, distilled water, or de-ionized water.

3.2 Bulk-Pore Volume Changes. Equation (10) can be rewritten as the ratio of the pore fluid volume change (ΔV_p) to the bulk volume change of the rock sample (ΔV), i.e.,

Table 1 Biot coefficient determined for different rocks from jacketed-unjacketed tests

				Jacketed test				Unjacketed test		
Rock	Pretest porosity Ø (%)	Equipment	$D \times L$ (mm)	σ (MPa)	Pore fluid	P (MPa)	K (GPa)	Ks (GPa)	α	Notes
Westerly granite [57]	1	Triaxial	—	0–240	Water	0	2.3∼43.9	45.5	0.04∼0.95	■ See text for details. ■ Jacketed test was conducted on a dry sample. ■ K and α were calculated by the authors of this review paper from the results presented in Fig. 3.
Flechtinger sandstone [62]	9.1–10.8	Triaxial	50 × 100	2–55	Water	1	2∼15	41.2	0.64–1.00	■ Sample was preconditioned by cycling σ between 0 and 60 MPa. Test temperatures varied between 30 °C and 120 °C.
Castlegate sandstone [63]	26	Triaxial	51 × 104	22–144	DI water	6.89	6.9–11.9	52.3–60.7	0.80–0.87	—
Berea sandstone [65,66]	23	True Triaxial	35 × 35 × 53	5–10	Water	0–5.0	7.9–13.3	29.4–30.9	0.71–0.74	■ Prismatic sample 35 × 35 × 53 mm. ■ Porosity measured under an isotropic stress of 5 MPa in a true triaxial cell.
Berea sandstone [67]	21	Triaxial	51 × 100	10–30	DI water	5–28.5	4.55	27.8	0.84	■ Sample was preconditioned by cycling σ between 20 and 40 MPa and P between 10 and 20 MPa.
Indo-Chinese granodiorite [68]	2.7	Triaxial	—	2–55	Water	2	2.5–8.2	19.5	0.55–0.87	■ Three samples tested: intact, with artificial vertical and horizontal fractures. ■ Samples preconditioned by three cycles of σ between 0 and 60 MPa ($P = 0$). ■ Test temperatures varied between 30 °C and 150 °C.
Callovo–Oxfordian claystone [69]	15.3–17.6	Triaxial	38 × 10	12–16	Water	4–6	2.0–3.0	21.7	0.87–0.91	■ α for a transversely isotropic case was also determined, which is discussed in Sec. 5.5.
Callovo–Oxfordian claystone [70]	17.9–18.2	Triaxial	38 × 10	10–14	Water	0–4	2.18	—	0.92	■ A synthetic pore water was used that had the same salinity as the in-situ fluid.
Opalinus clay [71]	13.3	Triaxial	38 × 12	4.5–8.0	Water	2.0	0.9	19.2	0.95	■ A synthetic pore water was used that had the same salinity as the Opalinus clay. ■ K_s was not measured but taken from other references. ■ α for the transversely isotropic case was determined (see Sec. 5.5).
Sorcy limestone [72]	28.4	Triaxial	60 × 125	22.5–27.5	Distilled water	5	13.2	83.0	0.84	■ Porosity was determined after the test.
Eau Claire shale [73]	10	Triaxial	30 × 60	0∼50	DI water	0	3.9–17.0	49.3	0.80	■ The reported α is for $\sigma' = 10$ MPa.
Opalinus clay [73]	13	triaxial	30 × 60	0-20	Water	0	1.7–2.7	8.9	0.70	■ In-situ brine was used for pore water.

Table 1 (continued)

Rock	Pretest porosity Ø (%)	Equipment	$D \times L$ (mm)	Jacketed test: σ (MPa)	Jacketed test: Pore fluid	Jacketed test: P (MPa)	Jacketed test: K (GPa)	Unjacketed test: Ks (GPa)	α	Notes
										The reported α is for $\sigma' = 10$ MPa.
Charcoal granite [73]	2	Triaxial	30×60	0∼50	DI water	0	9.7–46.4	63.2	0.71	■ The reported α is for $\sigma' = 10$ MPa.
Lac du Bonnet granite [74,75]	<0.5	Triaxial	58×153	0∼1.1	Distilled water	0	13.4	50.0	0.73	■ For the unjacketed test, the confining fluid (Syltherm 800 heat transfer fluid) was applied to the sample saturated with distilled water. ■ K_s is the average unjacketed modulus during loading and unloading under $\sigma = 2 - 22$ MPa.

Table 2 Biot coefficient determined for different rocks from bulk-pore volume changes

Rock	Pretest porosity Ø (%)	Equipment	$D \times L$ (mm)	σ (MPa)	Pore fluid	P (MPa)	ΔV_P (mm^3)	α	Notes
Flechtinger sandstone [62]	9.1–10.8	triaxial	50×100	2–55	Water	1	—	0.52–1	■ Sample was preconditioned by cycling confining stress between 0 and 60 MPa. ■ Temperature varied between 30 °C and 140 °C.
Berea sandstone [65]	23	Triaxial	$44 \times 87 \times 100$	0–5	Water	0	200	0.64–0.71	■ Prismatic sample $44 \times 87 \times 100$ mm. ■ Plane strain test in drained condition. ■ Porosity measured at $\sigma = 5$ MPa.
Sorcy limestone [72]	28.4	Triaxial	60×125	22.5–27.5	Distilled water	2–7	—	0.81	■ Porosity was determined after the test. ■ Two stress paths were followed: σ increased under constant P; P increased under constant σ.
Opalinus clay [80]	9.0–17.4	Oedometer	—	—	Water	—	—	0.8–0.95	■ A synthetic pore water was used, which had the same salinity as the Opalinus clay. ■ See text for measurement details. ■ Vertical effective stress varied from about 1 to 50 MPa.

Table 3 Biot coefficient determined for different rocks from isotropic-isochoric compression tests

Rock	Pretest porosity Ø (%)	Equipment	$D \times L$ (mm)	σ (MPa)	Pore fluid	P (MPa)	α	Notes
Bakken shale [81]	2.2–7.3	Core holder	25×50	22.9-27.1	Nitrogen	6.20–12.30	0.57–0.70	—
Bakken shale [82]	4.2–10.4	Triaxial	26×52	19.5-24.0	Nitrogen	6.0–12.0	0.58–0.87	—
Kansas chalk [85]	38.8	Triaxial	37×75	4.5∼17.5	Distilled water	0.7–14	0.92∼1	■ Axial stress was increased to suppress the axial strain (only) that occurred due to increased pore pressure.
Gosford sandstone [86]	17.6–18.9	Triaxial	38×64	28∼34	Brine	17∼27	0.84–0.91	■ Porosity measured at $\sigma = 3.6$ MPa.

$$\alpha = \frac{\Delta V_p}{\Delta V} \tag{27}$$

This technique only requires one drained isotropic compression test, which was discussed by many researchers [49,76–79]. This technique seems very attractive for high-porosity rocks where the entire pore space can be easily saturated, and the pore fluid is a single phase. The bulk volume change of a rock is conventionally measured using displacement sensors (e.g., strain gages, LVDTs, etc.); however, the pore volume change is equal to the volume of pore fluid drained out of the specimen subjected to isotropic compression. The latter measurement is extremely challenging for low-porosity rocks due to the minute volume of pore fluid drained during isotropic compression.

Reference [65] utilized this method for a sample of the Berea sandstone. The sample volume was about 380 mL. The pore volume change was very small (about 0.2 mL), drained from the test sample in the form of small drops, each measuring 0.02–0.03 mL in volume. Consequently, because of this uncertainty, they concluded that the calculated Biot coefficient was unreliable.

Reference [80] used a special case of Eq. (27) and estimated the Biot coefficient of the Opalinus clay under oedometric conditions (α_{oed}) where radial deformation (ε_r) is not permitted. Equation (28) was used for a transversely isotropic condition, where E_{oed} is the oedometric modulus (and equal to the increment of the total vertical stress divided by the increment of the corresponding volumetric strain after the induced pore pressure has completely dissipated), E_x and ν_{xy} are Young's modulus and Poisson's ratios in the direction parallel to the bedding plane, and E_z and ν_{zx} are the same parameters but in the direction perpendicular to the bedding plane. This method resulted in $\alpha_{\text{oed}} = 0.8 - 0.95$ for vertical effective stresses of about 1–50 MPa.

$$\alpha_{\text{oed}} = \frac{\Delta V_p}{\Delta V}\bigg|_{\varepsilon_r=0} = 1 - \frac{E_{\text{oed}}}{3K_s}\left[1 + \frac{2\nu_{zx}E_x}{E_z(1-\nu_{xy})}\right] \tag{28}$$

Table 2 summarizes the experimental details of the Biot coefficient measurements of the Flechtinger sandstone, Berea sandstone, Sorcy sandstone, and Opalinus clay using the bulk-pore volume changes method.

3.3 Isotropic–Isochoric Compression Test. The Biot coefficient can be determined by adjusting the confining stress (in the amount of $\Delta\sigma$) to prevent volume change (i.e., $\varepsilon_v = 0$) in the sample as a result of any variations in the pore pressure (ΔP). This relation can be derived from the definition of bulk modulus, that is

$$K = \frac{\Delta\sigma'}{\Delta\varepsilon_v} = \frac{\Delta(\sigma - \alpha P)}{\Delta\varepsilon_v} \tag{29}$$

Re-arranging for α, we find

$$\alpha = \frac{\Delta\sigma - K\Delta\varepsilon_v}{\Delta P} \tag{30}$$

For $\varepsilon_v = 0$, α is equal to

$$\alpha = \frac{\Delta\sigma}{\Delta P} \tag{31}$$

Only one drained isotropic compression test of a saturated sample is needed in this technique. However, a pressure feedback system is required such that the confining stress can be adjusted following a change in the pore pressure, in order to compensate for the sample volume change.

Theoretically, one could instead measure the change in pore pressure (ΔP) required to suppress the volume change of the sample imposed by a change in the confining stress ($\Delta\sigma$). This technique becomes disadvantageous when testing low-porosity rocks due to the long time required for deformation equilibrium.

He et al. [81] used this method in a core holder equipped with axial and radial strain gauges and measured α for the Bakken shale using Eq. (31); they determined the Biot coefficients of samples prepared parallel and perpendicular to the bedding plane.

Ling et al. [82] compared the Biot coefficient for nine cores of the Bakken shale, determined using this technique and the jacketed–unjacketed test method, both with the assumption that the material was isotropic.

Müller and Sahay [78] controversially argued that the effective stress coefficient determined from Eq. (27) can be different from those determined from Eqs. (15) or (31). The authors used the experimental data of the Berea sandstone reported in Ref. [83] and the Bentheimer sandstone from Ref. [84] and showed that (i) the results of Eq. (27) were generally lower than those from Eq. (15) for the Berea sandstone by a maximum difference of 0.25; (ii) they were higher for the Bentheimer sandstone for the range of simple effective stress studied (i.e., 0–70 MPa). These authors [78] argued that these differences were the impact of inhomogeneities at a small scale such as microcracks and other pore-scale features.

The details of the testing of the Bakken shale, Kansas chalk, and Gosford sandstone are provided in Table 3.

3.4 Matching Volumetric Strains of Dry and Saturated Samples. This technique was first proposed by Franquet and Abbas [87]. It does not require the measurement of the bulk or grain moduli. Drained isotropic compression tests are performed on two samples; a dry sample with zero pore pressure ($P = 0$) (called test 1) and a drained test on a saturated sample with variations in either σ or P (called test 2). The volumetric strains from test 1 are recorded and plotted as a function of the effective stress (which is equal to the total confining stress due to the lack of pore pressure). From test 2, the volumetric strains are plotted as a function of the pore pressure or confining stress. Assuming that: (i) the two samples are identical and (ii) water causes no (chemical) weakening effect on the saturated sample and there are no capillary forces at the interface of the fluid and the solid that could affect the elastic properties.

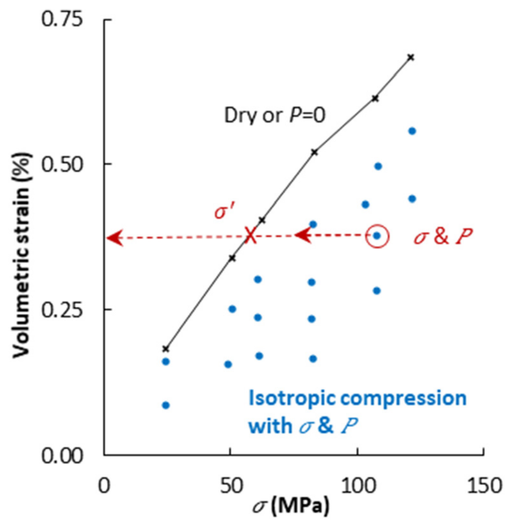

Fig. 4 Representation of the technique based on matching the volumetric strains of dry and saturated samples. Data are from tests on the Weber Sandstone conducted by Ref. [57], which were presented previously in Fig. 2. For any data point of σ and P, there is only one possible volumetric strain magnitude that corresponds to point X on the dry isotropic compression test data (black solid) curve; hence, α can be determined using Eq. (9).

By matching ε_v from the two tests, the corresponding α can be calculated for each pair of σ and P from Eq. (9). A graphic description of this approach is depicted in Fig. 4.

3.5 Estimation of Dry Bulk Modulus or Unjacketed Bulk Modulus. This method is based on the use of Eq. (15) but with an estimation of either the bulk or unjacketed modulus or both. Estimating K_s from the properties of the minerals of a rock avoids the long duration associated with measuring K_s from a conventional unjacketed test for low-porosity rocks.

For the low-porosity argillaceous Cobourg limestone from southern Ontario, Canada, Ref. [53] approximates $K_s =$ 66.0 GPa to 67.9 GPa from the volume fraction-based mineralogical compositions of the limestone determined from XRD measurements. The theoretical basis for estimating K_s was based on the theory of multiphasic elastic materials [88–91]. From an isotropic compression test on a dry cylindrical sample of the rock measuring 150 mm in diameter and 300 mm in length under $\sigma = 5 - 15$ MPa, Selvadurai [53] measured the bulk modulus as 22.73 GPa; hence, $\alpha = 0.66 - 0.67$.

Reference [60] used the mineralogical compositions and mineralogical elastic deformability properties reported in the literature and approximated the K_s of the Grimsel granite from Switzerland in order to estimate its Biot coefficient.

For the Lac du Bonnet granite obtained from the western region of the Canadian Shield, $K = 40.2$ GPa was estimated based on the Young's modulus and Poisson's ratio determined from UCS tests on relatively large samples ($D \times L = 100 \times 200$ mm and 150×300 mm) [61]. K_s was approximated as 58 MPa using the mineralogical composition of the rock from XRD. Consequently, the Biot coefficient was determined to be 0.3.

Reference [62] approximated the unjacketed modulus of the Flechtinger sandstone from its mineralogical composition as between 40.8 GPa and 41.8 GPa.

Compressional and shear wave velocities ($V_{P\text{wave}}$ and $V_{S\text{wave}}$, respectively) can be used to estimate the bulk modulus of a porous rock as shown in Eq. (32). In this equation, ρ_{dry} is the dry bulk density. Alam et al. [92] estimated the bulk modulus of the Valhall reservoir chalk in the North Sea using Eq. (32) while assuming that its grain modulus was equal to that of its constituent mineral (i.e., calcite)

$$K = \rho_{\text{dry}} \left(V_{P\text{wave}}^2 - \frac{4}{3} V_{S\text{wave}}^2 \right) \tag{32}$$

Reference [93] discusses a specific apparatus that can measure the bulk moduli for isotropic confining pressure oscillations over a broad frequency range. The authors summarized the bulk moduli and grain moduli (estimated from the mineralogical compositions) of several sandstones and limestones conducted by others: the Lavoux limestone [94], the Rustrel limestone [95], the Indiana limestone [95], the Vosgian sandstone [96], the Thuringen Sandstone [97], and the Fontainebleau Sandstone [98]. The rocks had porosity values in the range of 7%–24% and the estimated Biot coefficients were between 0.55 and 0.82.

According to Ref. [85], K estimated from Eq. (32) can differ from that measured using static techniques due to the difference in strain amplitudes. The other issue with ultrasonic testing is that at ultrasonic frequencies in saturated rock, the fluid pressure can be different from pore to pore; this lack of local fluid pressure equilibrium following application of the external load invalidates the conditions of the theory of poroelasticity [93]. As a result, the elastic moduli (including bulk modulus) at ultrasonic frequencies in saturated rock are different from those of the static conditions.

Furthermore, there are additional concerns regarding ultrasonic testing; determining mineralogical compositions from a thin section may not be an accurate volumetric representation of the rock.

3.6 Estimation of Biot Coefficient From Other Poroelastic Properties. The Biot coefficient is related to other fundamental poroelasticity parameters of a rock, including Skempton's pore pressure parameter (B), the drained bulk modulus of a porous rock (K), and the undrained bulk modulus (K_u), which are related through

$$\alpha = \frac{1}{B}\left(1 - \frac{K}{K_u}\right) \tag{33}$$

Measurements of the parameters B and K_u involve undrained triaxial experiments. Of particular significance in an undrained test is the calibration of the test results for compliance with the measuring system. It was shown by several researchers [69,72,95–101] that the compressibility of the water in the drainage system of a triaxial cell, as well as deformations of the pore pressure transducers, can have a substantial influence on reaching perfectly undrained conditions for measuring the poroelastic parameters (such as K_u). Similar to α, B is not a constant parameter; it decreases with an increase in simple effective stress [67,102–105].

Reference [72] determined $\alpha = 0.85$ for samples of the Sorcy limestone having a high porosity of 28.4%.

Reference [105] determined the Biot coefficient of Fontainebleau sandstone specimens ($\text{Ø} = 3 - 10\%$) based on the test results of the rock storage coefficient (s) using Eq. (34), under simple effective stresses up to 180 MPa. The values of α were determined to be between 0.25 and 0.85

$$\frac{\alpha}{KB} = s \tag{34}$$

3.7 Biot Coefficient as a Function of Bulk and Grain Compressibilities. Equation (15) can be rewritten in terms of the bulk and grain compressibilities as represented by Eq. (35) [77,79,106,107] where C_b and C_s are the compressibility of the bulk material (in a dry or drained condition) and the solid grains, respectively. C_b and C_s can be determined from the jacketed and unjacketed tests as described in Sec. 3.1 and are equal to inverse values of K and K_s, respectively (see Fig. 3)

$$\alpha = 1 - \frac{C_s}{C_b} \tag{35}$$

4 Other Interpretations of Effective Stress Coefficients and Their Measurements

Following a general effective stress framework similar to Biot's effectives stress proncipile, scholars from various disciplines have defined and measured effective stress coefficients for conditions such as failure state or permeability hysteresis which do not comply with Biot's linear isotropic poroelasticty. They considered a factor for the pore pressure term in their effective stress definitions, called the effective stress (or effective pressure) coefficient. Several developments from this category are discussed in the Secs. 4.1–4.5.

4.1 Effective Stress Coefficient for the Failure State—Matching Failure Envelopes of Dry and Saturated Samples. This technique has been used by many researchers, for example, Refs. [87] and [108]. Several triaxial compression tests on dry samples are conducted under various confining stresses; therefore, a Mohr–Coulomb envelope can be constructed for the effective stress (pore pressure is zero). By performing an additional triaxial test with nonzero pore pressure, and assuming that (i) there is no heterogeneity among the samples and (ii) water causes no (chemical) weakening effect on the saturated sample and there are no capillary forces at the interface of the fluid and the solid that could affect the elastic properties, the effective stress coefficient for the failure state, α_f, can be determined by substituting the effective stress definition of Eq. (9) into the Mohr–Coulomb failure criterion (Eq. (36)). This can be done using the graphical approach shown in Fig. 5. By knowing $\sigma_1 - \sigma_3$ from the tests on the saturated sample, a circle is drawn and shifted to the left of the diagram until it touches the Mohr–Coulomb failure envelope (i.e., the material exhibits elastic behavior up to the development of failure). It is worth noting that the saturated and dry specimens should be tested within the same stress ranges in order to obviate the nonlinearity issue of the failure envelope.

$$\alpha_f = \frac{\sigma_1 + \sigma_3}{2P} - \frac{\sigma_1 - \sigma_3}{2P \sin\varphi} + \frac{c}{P}\cot\varphi \tag{36}$$

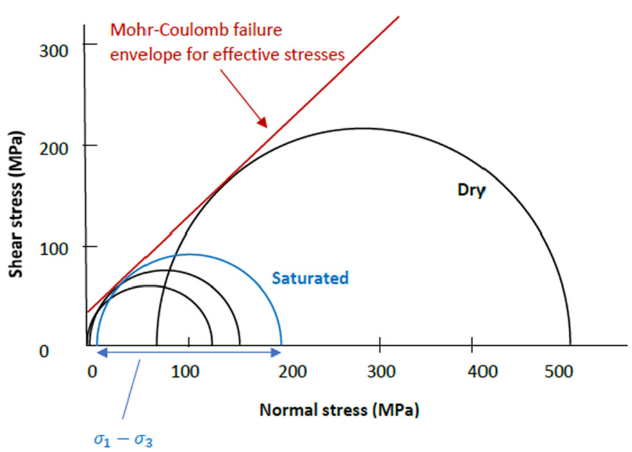

Fig. 5 Estimating the effective stress coefficient of a sandstone by constructing a Mohr–Coulomb failure envelope using the results from several triaxial strength tests on dry samples under different stress conditions (black Mohr circles) and one triaxial strength test on a saturated sample of the same rock with $P \neq 0$ (blue Mohr circle). The data was taken from Ref. [87].

In Eq. (36), the parameters c and φ are the cohesion and friction angle, respectively, and σ_1 and σ_3 are the maximum and minimum principal stresses, respectively.

If ψ is defined as the slope of the failure envelope in the $\sigma_1' - \sigma_3'$ plane and the unconfined compressive strength of the rock is represented by UCS, then α_f can be expressed as

$$\alpha_f = \frac{\sigma_1 - \text{UCS} - \sigma_3 \tan\psi}{P(1 - \tan\psi)} \tag{37}$$

Using a similar approach, Ref. [108] determined the α_f for the peak and residual strength of rock; no clear relationship between the two was observed.

Baud et al. [109] conducted triaxial strength tests on samples of the Bleurswiller sandstone and concluded that using a linear fit to the differential stress versus $\sigma - \alpha_f P$ for the brittle regime resulted in an effective stress coefficient of about 0.95 for the sandstone. These authors [109] reported that the brittle failure of wet samples occurred at a significantly lower stress than in dry samples (i.e., water weakening effect).

The failure envelope method might seem simpler than others as it does not include any compressibility measurements. However, unlike the original Biot theory, the sample undergoes anisotropic stresses, and the pore pressure response is expected to be different from that under isotropic compression. This is because, while the material is subjected to a deviator stress that approaches failure, damage evolution results in the generation of new cracks and changes to the pore network. Consequently, this technique is intended to determine α_f for peak and residual strengths, which are expected to be distinctly different from Biot coefficient calculated using Eqs. (15), (27), (31), (33), (34), and (35). A review of the experimental data of a wide variety of rocks is given in Ref. [104], and it concluded that Terzaghi's effective stress generally governs the shear failure of rocks where $\alpha_f = 1$ can be assumed, although there are exceptions.

4.2 Effective Stress Coefficient From Variations of Permeability With Pore Pressure and Confining Stress. There are several measurement interpretation techniques published in the literature for the effective stress coefficient based on rock permeability measurements (α_k); these are discussed below. Each technique is assigned a different subscript for α_k.

4.2.1 Trial-and-Error Method. This technique involves measuring the permeability (k) of a rock at various P and σ combinations. By assuming an initial effective stress coefficient of $\alpha_{k.\text{trial}}$, the results are plotted as a function of σ', for several constant P values. $\alpha_{k.\text{trial}}$ is then varied until all curves merge into one curve or into a narrow band. It should be noted that this method yields a single value of $\alpha_{k.\text{trial}}$ for the entire spectrum of P and σ, and consequently σ'.

A transient method following the pressure transmission technique (proposed by Refs. [110] and [111]) measured the permeability of a carbonate rock to nitrogen. After attaining equilibrium at a predefined value of pore pressure, only the upstream pressure was instantaneously raised. The downstream gas pressure buildup was monitored as a function of time until it equaled the upstream gas pressure again. The resulting data was used to determine k and $\alpha_{k.\text{trial}}$. As depicted in Fig. 6, when $\alpha_{k.\text{trial}} = 1.0$ all data from the various pore pressure values merged into a single curve; hence, this value can be regarded as the most representative value of the effective stress coefficient for permeability of this rock.

The details of determining the effective stress coefficient of the Niobrara shale and a carbonate rock sample using the trial-and-error method are provided in Table 4.

4.2.2 Partial Derivatives of Permeability with Respect to Pore Pressure and Confining Stress. Several researchers used a fundamental assumption that certain properties of rocks, such as k, ε_v, $V_{P\text{wave}}$, are functions of the effective stress [82,112–114]. As

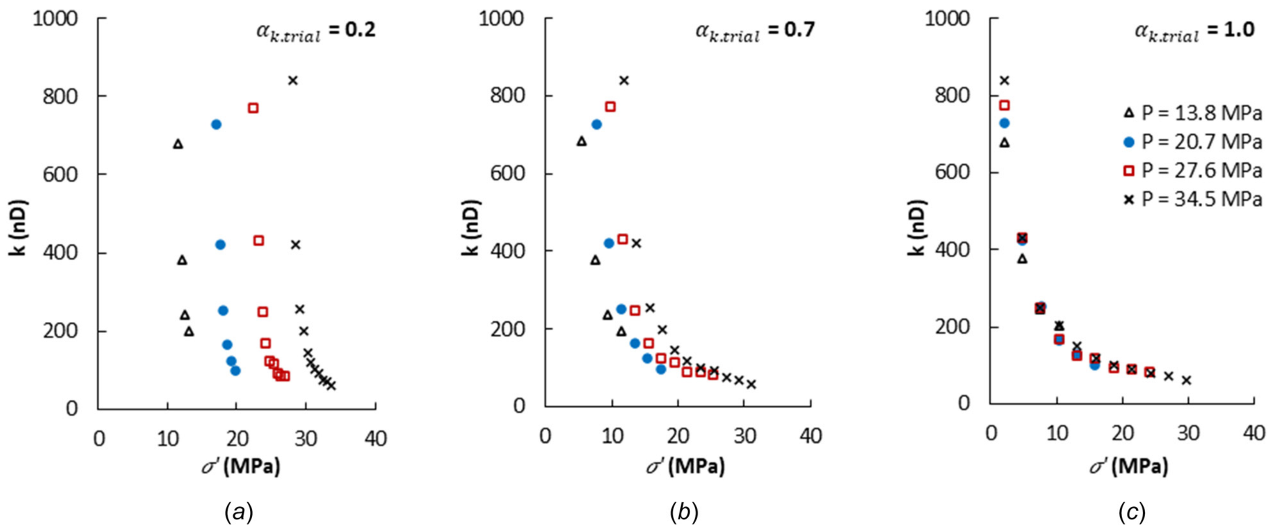

Fig. 6 Trial-and-Error method for determining $\alpha_{k.\mathrm{trial}}$ of a carbonate rock from its permeability. If a correct $\alpha_{k.\mathrm{trial}}$ is selected, all curves merge into one curve or a narrow band. The experimental dataset is for the carbonate rock given in Ref. [111].

a result, variations of a parameter q will consist of the contributions from the constituents of σ', i.e., σ and P (Eq. (38))

$$dq = \frac{\partial q}{\partial \sigma} d\sigma + \frac{\partial q}{\partial P} dP \tag{38}$$

At a constant σ', Eq. (39) is satisfied; hence, q will not experience any variations,

$$d\sigma' = 0 \rightarrow d\sigma = \alpha_{q.\mathrm{der}.P\&\sigma} dP \tag{39}$$

Substituting Eq. (39) into Eq. (38) yields Eq. (40). In this equation, $\frac{\partial q}{\partial P}$ represents the variation of q as a result of changing P while σ remains unchanged. The parameter $\frac{\partial q}{\partial \sigma}$ indicates a variation of q corresponding to a change in σ while P is kept constant. Rewriting Eq. (40) for permeability (k) gives Eq. (41)

$$\alpha_{q.\mathrm{der}.P\&\sigma} = -\frac{\frac{\partial q}{\partial P}}{\frac{\partial q}{\partial \sigma}} \tag{40}$$

$$\alpha_{k.\mathrm{der}.P\&\sigma} = -\frac{\frac{\partial k}{\partial P}}{\frac{\partial k}{\partial \sigma}} \tag{41}$$

In reference [102] the permeability of the Stainton sandstone was measured as a function of pore pressure and at two constant confining stresses of 10 and 20 MPa. As depicted in Fig. 7, the two permeability curves corresponding to $\sigma = 10$ MPa and $\sigma = 20$ MPa were found to be approximately 1.84 MPa apart on the $k - P$ coordinate plane (i.e., $\Delta P = 1.84$ MPa); using Eq. (39) resulted in $\alpha_{k.\mathrm{der}.P\&\sigma} = 5.4$ for the sandstone.

Using Eq. (41) [112] estimated $\alpha_{k.\mathrm{der}.P\&\sigma}$ to be in the range of 0.3 to 0.85 for the Chelmsford granite as plotted in Fig. 8. Since this method includes loading-unloading cycles, the resulting values of $\alpha_{k.\mathrm{der}.P\&\sigma}$ will be representative of various states of effective stress. Equation (41) was used by other researchers, e.g., Refs. [115] and [116].

The details of tests on the Stainton sandstone, Pottsville sandstone, Pigeon Cove granite, Westerly granite, Chelmsford granite, and Barre granite are summarized in Table 4.

4.2.3 Response Surface and Variations of Transformed Permeability. This method also involves measuring the permeability of a rock at various confining stress and pore pressure combinations. The response surface approach proposed by Ref. [119] can then be used to fit a surface to a set of data (here, permeability, k) that are dependent on the two variables (here σ and P). This approach was utilized by several researchers [114,117,120]. To yield a smooth surface, a linear or second-degree polynomial surface can be fitted to the transformed permeability (k^λ) data. A quadratic response surface of $k^\lambda - \sigma - P$ is defined by Eq. (42), where λ varies from –3 to +3, with $\lambda = 0$ representing the natural log transformation

$$k^\lambda = a_1 + a_2\sigma + a_3 P + a_4\sigma^2 + a_5\sigma P + a_6 P^2 \tag{42}$$

where the coefficients a_1 through a_6 are calculated by a least squares regression analysis. Once these coefficients are determined, substituting k^λ from Eq. (42) into Eq. (40) will yield a three-dimensional surface for the effective stress coefficient on the $\alpha_{k.\mathrm{tran}.P\&\sigma} - \sigma - P$ surface (Eq. (43))

$$\alpha_{k.\mathrm{tran}.P\&\sigma} = -\frac{a_3 + a_5\sigma + 2a_6 P}{a_2 + 2a_4\sigma + a_5 P} \tag{43}$$

Reference [114] determined the transformed permeability response surface for samples of the Ekofisk chalk having a 15% porosity. The authors proposed a natural log transformation form for both loading and unloading cycles and fitted the quadratic response surfaces of Eq. (43) to the permeability data.

In Ref. [121] Eq. (43) is used for k^λ data from the Austin chalk and Saratoga limestone samples.

Li et al. [120] utilized Eq. (43) to estimate $\alpha_{k.\mathrm{tran}.P\&\sigma}$ for the E-bei sandstone. Their calculations resulted in values less than zero and value greater than unity. They found that these extreme and unsatisfactory values occurred at the boundaries of the $\sigma - P$ domain. They concluded that the negative values, and values smaller than the porosity of the rock, are not physically possible. Eventually, they concluded that the most satisfactory values might be between 0.06 and 0.86.

Experimental data of the effective stress coefficient measurements for the Northern Hubei sandstone using this technique are summarized in Table 4.

4.2.4 Cubic Root Equation. Reference [118] introduced Eq. (44) for the permeability of the Westerly granite. In this equation, A and B are two constants that depend on the geometric parameters of the cracks in the rock, and $\alpha_{k.\mathrm{cubic}}$ is the effective stress coefficient from this method. Differentiation of Eq. (44) with respect to pore pressure delivers Eq. (45). Experimental data for the effective stress coefficient of the Westerly granite using

Table 4 Effective stress coefficient determined for different rocks from permeability variation techniques

Rock	Pretest porosity Ø (%)	Equipment	k technique	$D \times L$ (mm)	σ (MPa)	Pore fluid	P (MPa)	k (m^2)	α_k equation no.	α_k	Notes
Trial-and error ($\alpha_{k.\mathrm{trial}}$)											
Niobrara shale [111]	2–5.5	Core holder	Pressure transmission	38 × 48	13.8–34.5	Nitrogen	3.4–32.4	20–45	Trial-and-error	0.8	■ Matrix (intact) sample. ■ Porosity determined under $\sigma = 3.4 - 13.8$ MPa. ■ Permeability in Nano-Darcy (nD).
Niobrara shale [111]	—	Core holder	Pressure transmission	38 × 25	13.8–34.5	Nitrogen	3.4–32.4	200–2500	Trial-and-error	1.0	■ Sample with sealed fractures. ■ Permeability in Nano-Darcy (nD).
Carbonate [111]	—	Core holder	Pressure transmission	38 × 35	13.8–34.5	Nitrogen	3.4–32.4	100–900	Trial-and-error	1.0	■ Permeability in Nano-Darcy (nD). ■ Test results are plotted in Fig. 6.
Partial derivatives of permeability with respect to pore pressure and confining stress ($\alpha_{k.\mathrm{der}.P\&\sigma}$)											
Stainton sandstone [102]	16	Triaxial	—	38 × 78	10–20	Water	2–15	10.8–11.8	41	5.4	■ Permeability in milli Darcy (mD). See text for details.
Pottsville sandstone [112]	—	—	Pulse decay	19 × 25	40–200	Distilled water	10–30	10^{-20}–10^{-19}	41	0.2–1.1	■ Range of $\alpha_{k.\mathrm{der}.P\&\sigma}$ for several loading-unloading cycles.
Pigeon Cove granite [112]	—	—	Pulse decay	19 × 25	40–160	Distilled water	10–30	10^{-20}–10^{-19}	41	0.3–1.2	■ Range of $\alpha_{k.\mathrm{der}.P\&\sigma}$ for several loading-unloading cycles.
Westerly granite [112]	—	—	Pulse decay	19 × 25	20–120	Distilled water	10–30	10^{-22}–10^{-20}	41	0.4–0.8	■ Range of $\alpha_{k.\mathrm{der}.P\&\sigma}$ for several loading-unloading cycles.
Chelmsford Granite [112]	—	—	Pulse decay	19 × 25	40–180	Distilled water	10–30	10^{-20}–10^{-18}	41	0.3~0.9	■ Range of α for several loading-unloading cycles. ■ Test results are plotted in Fig. 8.
Barre Granite [112,113]	—	—	Pulse decay	19 × 25	40–160	Distilled water	10–30	10^{-20}–10^{-19}	41	0.43–0.85	■ Range of α for several loading-unloading cycles.
Response surface and variations of transformed permeability ($\alpha_{k.tran.P\&\sigma}$)											
Northern Hubei sandstone [117]	2.4–5.5	—	Steady state	25 × 40	12–44	Nitrogen	6–25	2×10^{-16}	41 and 42 ($\lambda = 0$)	0.01–0.98	■ Range of $\alpha_{k.\mathrm{tran}.P\&\sigma}$ for all loading-unloading cycles.
Cubic root equation ($\alpha_{k.cubic}$)											
Westerly granite [118]	—	Triaxial	Steady state	25 × 25	11–96	DI water	1–86	10^{-21}–10^{-19}	44 and 45	0.95–1.23	■ Range of $\alpha_{k.\mathrm{cubic}}$ for 3 loading-unloading cycles. ■ Range of $\alpha_{k.\mathrm{cubic}}$ for differential method of Eq. (44) and graphical method of Eq. (45).

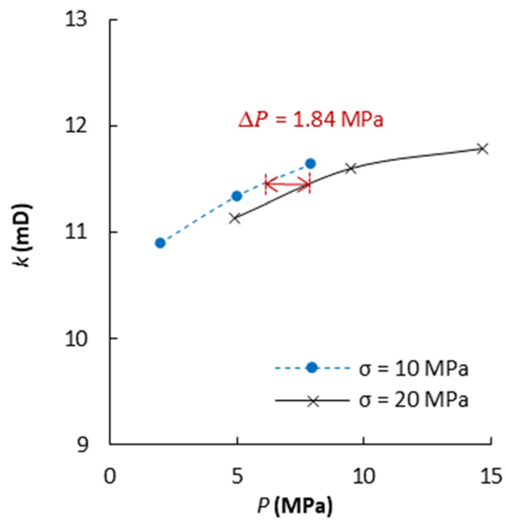

Fig. 7 Permeability of the Stainton sandstone as a function of pore pressure at confining stresses of 10 MPa and 20 MPa. The $\Delta P = 1.84$ MPa offset between the two curves resulted in $\alpha_{k.\mathrm{der}}.P\&\sigma = 5.4$ for the sandstone [102].

this graphical technique are summarized in Table 4. There is a second method for finding $\alpha_{k.\mathrm{cubic}}$ from Eq. (44); rearranging Eq. (45) results in Eq. (46). The plot of the pore pressure as a function of the partial derivative term gives a straight line with a slope B and intercept $\frac{\sigma}{\alpha_{k.\mathrm{cubic}}}$. As depicted in Fig. 9, the cubic root of the permeability data is plotted as a function of the effective stress, where $\alpha_{k.\mathrm{cubic}} = 1.0$ results in the least deviation from a straight line.

$$k^{\frac{1}{3}} = A + B\ln(\sigma - \alpha_{k.\mathrm{cubic}}P) \tag{44}$$

$$\frac{\partial(k^{\frac{1}{3}})}{\partial P} = -\frac{B\alpha_{k.\mathrm{cubic}}}{\sigma - \alpha_{k.\mathrm{cubic}}P} \tag{45}$$

$$P = B\frac{\partial P}{\partial(k^{\frac{1}{3}})} + \frac{\sigma}{\alpha_{k.\mathrm{cubic}}} \tag{46}$$

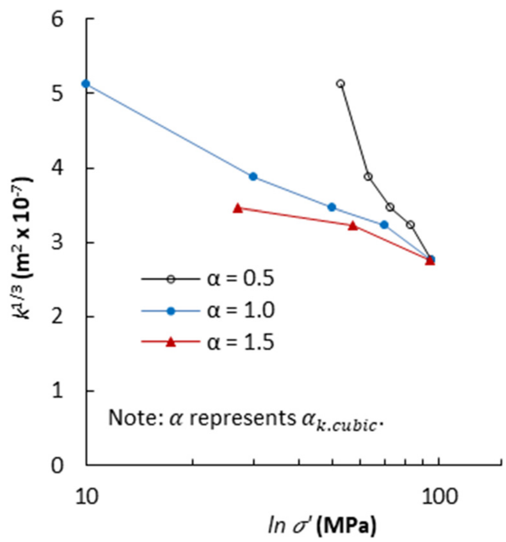

Fig. 9 The graphical method for determining $\alpha_{k.\mathrm{cubic}}$ for the Westerly granite from the cubic root permeability equation. The data is taken from to the first loading cycle at a confining stress of 96 MPa. $\alpha_{k.\mathrm{cubic}}$ is varied until the curve approaches a straight line [118].

4.3 Effective Stress Coefficient From Variations of Deformation With Pore Pressure and Confining Stress

4.3.1 Partial Derivatives of Deformation with Respect to Pore Pressure and Simple Effective Stress. This technique is based on the fundamental assumption that a physical property of a rock is a function of the effective stress. Unlike Sec. 4.2.2, this approach assumes that variations of a parameter q will be composed of the contributions from the simple effective stress (or differential pressure) and pore pressure. Similar to Eq. (40) but taking the derivatives of q with respect to P and σ'_s, the effective stress coefficient from this method, $\alpha_{q.\mathrm{der}.P\&\sigma'_s}$, is determined using Eq. (47)

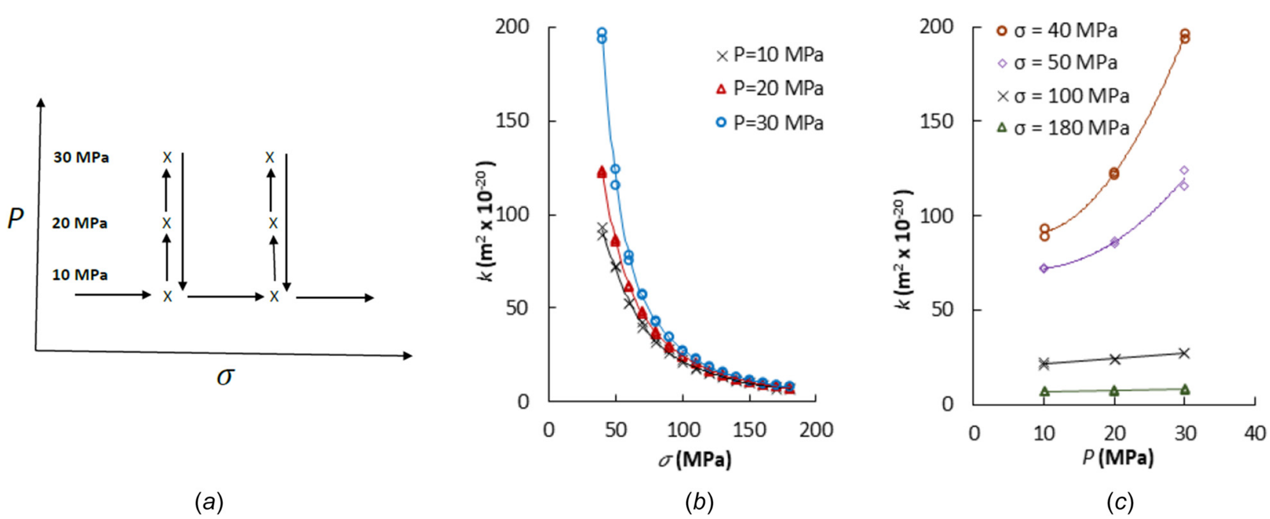

Fig. 8 Determination of $\alpha_{k.\mathrm{der}}.P\&\sigma$ for the Chelmsford granite from variations in permeability due to pore pressure and confining stress [102]: (*a*) loading scheme; (*b*) variations of permeability as a function of confining stress under different constant pore pressure values; and (*c*) variations of permeability as a function of pore pressure under different constant confining stress values

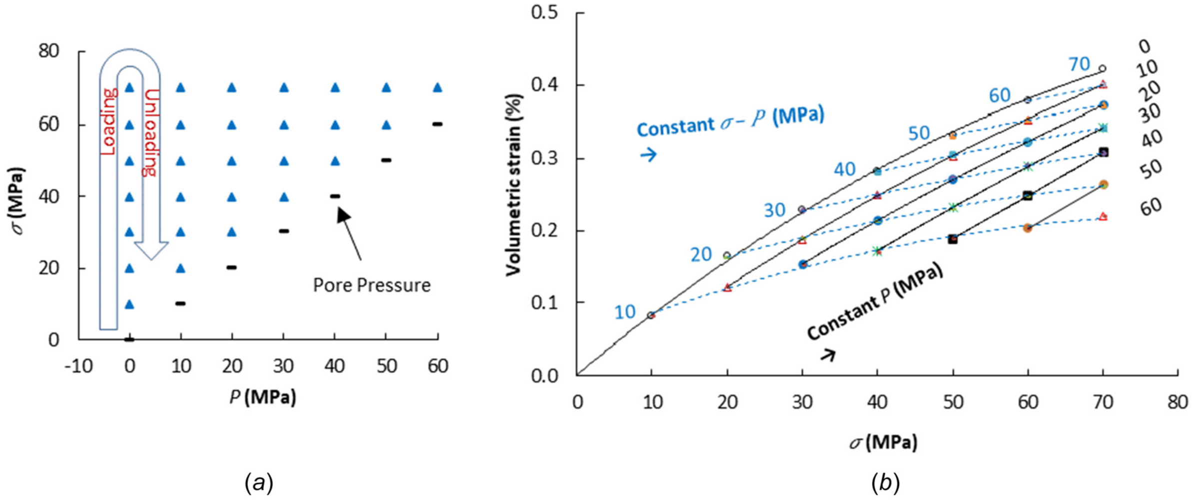

Fig. 10 (*a*) loading scheme and (*b*) variations in volumetric strain of the Bakken shale (Ø = 7.1%) with pore pressure and simple effective stress. The ratio of slopes at each intersection point of the constant P and constant $\sigma - P$ lines was calculated and substituted in Eq. (48); $\alpha_{\varepsilon_v.\mathrm{der}.P\&\sigma'_s}$ was estimated between 0.25 to 0.95 for the loading path (data from Ref. [122]).

$$\alpha_{q.\mathrm{der}.P\&\sigma'_s} = 1 - \frac{\dfrac{\partial q}{\partial P}}{\dfrac{\partial q}{\partial \sigma'_s}} \tag{47}$$

Reference [122] extended Eq. (47) to volumetric strain as represented by Eq. (48) and used it in testing the Bakken shale samples; the test results are shown in Fig. 10

$$\alpha_{\varepsilon_v.\mathrm{der}.P\&\sigma'_s} = 1 - \frac{\dfrac{\partial \varepsilon_v}{\partial P}}{\dfrac{\partial \varepsilon_v}{\partial \sigma'_s}} \tag{48}$$

Nermoen et al. [85] took a similar approach and determined the effective stress coefficient from the derivatives of the axial strain (ε_a) due to ramping σ'_s and P (Eq. (49))

$$\alpha_{\varepsilon_a.\mathrm{der}.P\&\sigma'_s} = 1 - \frac{\dfrac{\partial \varepsilon_a}{\partial P}}{\dfrac{\partial \varepsilon_a}{\partial \sigma'_s}} \tag{49}$$

The details of estimation of the effective stress coefficients of the Kansas chalk, Ekofisk chalk, and Bakken cores are summarized in Table 5.

4.3.2 Response Surface and Variations of Transformed Volumetric Strain. By fitting a quadratic response surface to the transformed volumetric strain (ε_v^λ) data of the Ekofisk chalk, Ref. [114] suggested that $\varepsilon_v^\lambda - \sigma - P$ has the form of Eq. (50) and the corresponding effective stress coefficient $\alpha_{\varepsilon_v.\mathrm{tran}.P\&\sigma}$ can be determined from Eq. (51). The parameter λ for the loading and unloading cycles of three samples with porosity values of 15%, 24%, and 36% were between 1.0 and 2.6 and. The $\alpha_{\varepsilon_v.\mathrm{tran}.P\&\sigma}$ at all average confining stresses and pore pressures were between 0.74 and 1.03. The experimental results of the 36% porosity sample are shown in Fig. 11 and all sample results are summarized in Table 5.

Reference [121] also applied Eq. (50) to ε_v^λ data from the Austin chalk and Saratoga limestone samples

$$\varepsilon_v^\lambda = a_1 + a_2\sigma + a_3P + a_4\sigma^2 + a_5\sigma P + a_6P^2 \tag{50}$$

$$\alpha_{\varepsilon_v.\mathrm{tran}.P\&\sigma} = -\frac{a_3 + a_5\sigma + 2a_6P}{a_2 + 2a_4\sigma + a_5P} \tag{51}$$

4.4 Effective Stress Coefficient From Partial Derivatives of Geophysical Properties With Respect to Pore Pressure and Simple Effective Stress. Todd and Simmons [123] introduced Eq. (52) for the effective stress coefficient based on experimental data of compressional wave velocity ($V_{P\mathrm{wave}}$). Similarly, the effective stress coefficient can be written as in Eqs. (53) and (54) based on shear wave velocity ($V_{S\mathrm{wave}}$) and the attenuation factor (Q_P), respectively.

Reference [124] used Eq. (52) for $V_{P\mathrm{wave}}$ and Eq. (54) for Q_P; they used each set of geophysical measurements in a true triaxial apparatus to determine the effective stress coefficient of the Berea sandstone and Michigan sandstone

$$\alpha_{V_{P\mathrm{wave}}.\mathrm{der}.P\&\sigma'_s} = 1 - \frac{\dfrac{\partial V_{P\mathrm{wave}}}{\partial P}}{\dfrac{\partial V_{P\mathrm{wave}}}{\partial \sigma'_s}} \tag{52}$$

$$\alpha_{V_{S\mathrm{wave}}.\mathrm{der}.P\&\sigma'_s} = 1 - \frac{\dfrac{\partial V_{S\mathrm{wave}}}{\partial P}}{\dfrac{\partial V_{S\mathrm{wave}}}{\partial \sigma'_s}} \tag{53}$$

$$\alpha_{Q.\mathrm{der}.P\&\sigma'_s} = 1 - \frac{\dfrac{\partial Q_P}{\partial P}}{\dfrac{\partial Q_P}{\partial \sigma'_s}} \tag{54}$$

Mulchandani and Sharma [125] used the $V_{P\mathrm{wave}}$ and $V_{S\mathrm{wave}}$ measured by Ref. [126] on carbonate samples (saturated with brine or butane) and determined the effective stress coefficients using Eqs. (52) and (53), respectively.

Variations of $V_{P\mathrm{wave}}$ for prismatic samples of the Gosford sandstone under different isotropic confining stresses and pore pressures were measured in a true triaxial apparatus [127]; using Eq. (52) the effective stress coefficient was determined to be between 0.92 and 0.98 for $\sigma = 4.2 - 6.8$ MPa.

Table 5 Effective stress coefficient determined for different rocks from deformation variation techniques

Rock	Pretest porosity Ø (%)	Equipment	$D \times L$ (mm)	σ (MPa)	Pore fluid	P (MPa)	$\alpha_{\varepsilon.P\&\sigma_s'}$ equation no.	$\alpha_{\varepsilon.P\&\sigma_s'}$	Notes
Partial derivatives of deformation with respect to pore pressure and simple effective stress ($\alpha_{\varepsilon.P\&\sigma_s'}$)									
Kansas chalk [85]	38.1	Oedometer	23×38	3–21	Distilled water	1.5–19.5	49	0.85∼0.98	■ Values reported under σ are axial stresses. ■ $\alpha_{\varepsilon_a.\text{der}.P\&\sigma_s'}$ was determined based on variations of axial strain.
Bakken cores [122]	3.7–14.4	Triaxial	25×25	10–70	Argon	0–60	48	0.25–0.95	■ Horizontal and vertical samples from lime-wackestone, fine sandstone, lime-packstone, and dolomite sediment. ■ Three small holes 8.5 mm deep and 1 mm in diameter were drilled on each end of the specimen to speed up saturation. ■ $\alpha_{\varepsilon_v.\text{der}.P\&\sigma_s'}$ was determined based on variations of volumetric strain.
Response surface and variations of transformed volumetric strain ($\alpha_{\varepsilon_v.\text{tran}.P\&\sigma}$)									
Ekofisk chalk [114]	15–36	Triaxial	25×56	6.9–55.2	Nitrogen	6.9–27.6	50 and 51 ($\lambda = 1.0 - 2.6$)	0.74–1.03	■ Three samples with porosities of 15%, 24%, and 36% were tested. ■ Samples were seasoned by cycling to the maximum target confining stress. ■ $\alpha_{\varepsilon_v.\text{tran}.P\&\sigma}$ was determined based on variations of volumetric strain. ■ Range of $\alpha_{\varepsilon_v.\text{tran}.P\&\sigma}$ for loading and unloading paths of all three samples. ■ See the results of the 36% porosity sample in Fig. 11.

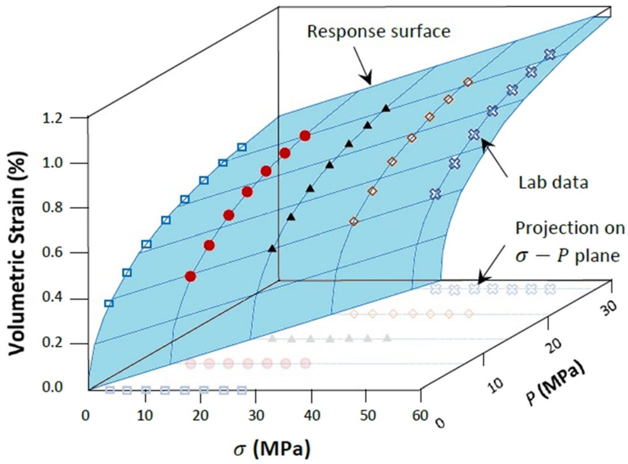

Fig. 11 Transformed response surface of volumetric strain of the Ekofisk chalk (Ø = 36%) as a function of confining stress and pore pressure; the projected points are estimated from the original figure in Ref. [114]. Teufel and Warpinski [114] determined $\alpha_{\varepsilon_v.\mathrm{tran}}.P\&\sigma$ equal to 0.96 for the loading path shown here.

Other researchers [128–130] also estimated the effective stress coefficient using Eqs. (52) and (53). Several case studies from the literature are reported in Table 6, including tests on the Berea sandstone, Michigan sandstone, Juan de Fuca ridge basalt, and Oman dolerite.

4.5 Effective Stress Coefficient as a Function of Bulk, Grain, and Pore Compressibilities. Geertsma [133] rederived the effective stress coefficient in terms of compressibilities of bulk and pore volume as a consequence of changes in total stress and pore pressure. As discussed by Ref. [106], there are four different compressibilities for a porous rock, which can be associated with changes in either the bulk volume (V_b) or pore volume (V_p) as a result of changes in either confining stress or pore pressure as defined in Eqs. (55)–(58). $C_{b\sigma}$ and C_{bP} represent the bulk compressibilities induced by variations of confining stress and pore pressure, respectively. $C_{P\sigma}$ and C_{PP} are the pore compressibilities caused by changes in confining stress and pore pressure, respectively,

$$C_{b\sigma} = \frac{1}{V_b}\left(\frac{\partial V_b}{\partial \sigma}\right) \tag{55}$$

$$C_{bP} = -\frac{1}{V_b}\left(\frac{\partial V_b}{\partial P}\right) \tag{56}$$

$$C_{P\sigma} = \frac{1}{V_b}\left(\frac{\partial V_P}{\partial \sigma}\right) \tag{57}$$

$$C_{PP} = -\frac{1}{V_b}\left(\frac{\partial V_P}{\partial P}\right) \tag{58}$$

In Ref. [106] it was shown that

$$C_{bP} = C_{b\sigma} - C_s \tag{59}$$

$$C_{bP} = ØC_{P\sigma} \tag{60}$$

$$C_{PP} = C_{P\sigma} - C_s \tag{61}$$

$$C_{P\sigma} = \frac{C_{b\sigma} - C_s}{Ø} \tag{62}$$

$$C_{PP} = \frac{[C_{b\sigma} - C_s(1+Ø)]}{Ø} \tag{63}$$

Table 6 Effective stress coefficient determined for different rocks from geophysical property variation techniques

Rock	Pretest porosity Ø (%)	Equipment	$D \times L$ (mm)	σ (MPa)	Pore fluid	P (MPa)	Based on $V_{P\mathrm{wave}}$	Based on $V_{S\mathrm{wave}}$	Based on Q_P	Notes
Berea Sandstone [124]	21.2	True triaxial	18 × 18 × 18	5–25	Brine	—	0.78–0.99	—	0.81–1.10	■ Prismatic sample 18 × 18 × 18 mm. ■ Reported α represent cases where $P = 0$ and $P \neq 0$.
Michigan sandstone [124]	16.9	True triaxial	18 × 18 × 18	5–25	Brine	—	0.62–0.98	—	0.70–0.86	■ Prismatic sample 18 × 18 × 18 mm. ■ Reported α represent cases where $P = 0$ and $P \neq 0$.
Berea sandstone [131]	19.2	Triaxial	25 × 33	0.5–100	Distilled water	0	0.84–0.99	1.02–1.17	—	—
Juan de-Fuca ridge basalt [132]	4.0	Triaxial	25 × 50	0–140	Water	0–120	0.75–0.90	0.91–0.99	—	—
Oman dolerite [132]	1.1	Triaxial	—	0–140	Water	0–120	0.64–0.92	0.76–0.93	—	—

Table 7 Effective stress coefficient determined for different rocks from bulk-pore compressibilities

Rock	Pretest porosity Ø (%)	Equipment	$D \times L$ (mm)	σ (MPa)	Pore fluid	P (MPa)	α_b or α_P	Effective stress coefficient	Notes
Bakken shale [82]	4.2–10.4	Triaxial	26×52	—	Nitrogen	—	α_b	0.55–0.91	—
Boise sandstone [106]	25.6	Triaxial	51×51	2∼40	Brine	1.5∼15.5	α_P	1.02	■ See text for details.
Berea sandstone [106]	22.2	Triaxial	51×51	2∼40	Brine	1.5∼15.5	α_P	1.02	■ See text for details.
Bandera sandstone [106]	16.5	Triaxial	51×51	2∼40	Brine	1.5∼15.5	α_P	1.06	■ See text for details.

Hence, two effective stress coefficients can be defined as follows:

$$\alpha_b = \frac{C_{bP}}{C_{b\sigma}} = 1 - \frac{C_s}{C_{b\sigma}} \tag{64}$$

$$\alpha_P = \frac{C_{PP}}{C_{P\sigma}} = 1 - \frac{ØC_s}{C_{b\sigma} - C_s} = 1 - \frac{C_s}{C_{P\sigma}} \tag{65}$$

Zimmerman et al. [106] analytically proved that the effective stress coefficient determined from variations of the pore volume (α_P) is always greater than the effective stress coefficient estimated from changes in the bulk volume (α_b). They also derived Eqs. (66) and (67) as the bounds for α_b and α_P, respectively. Compared to Eq. (26), Eq. (66) tends to overestimate the lower limit of the effective stress coefficient

$$\frac{3Ø}{2+Ø} \le \alpha_b \le 1 \tag{66}$$

$$\frac{1+2Ø}{3} \le \alpha_P \le 1 \tag{67}$$

In reference [61], Eq. (66) was used to estimate the Biot coefficient for the Lac du Bonnet granite with a porosity of $Ø = 0.7\%$. The effective coefficient estimated from Eq. (66) was 0.01, which was significantly lower than the experimentally derived value of $\alpha = 0.30$. Selvadurai [61] also observed that the Biot coefficient is rarely below 0.2 for the low porosity range of 2–15%.

Three sandstones (Boise sandstone, Berea sandstone, Bandera sandstone) were tested in a triaxial apparatus [106] and measured the variations of $C_{P\sigma}$ and C_{bP} under different confining stresses and pore pressures were measured. $C_{P\sigma}$ values were plotted versus effective stress and under several constant pore pressures; once an optimal value for the effective stress coefficient of each rock was used, the different $C_{P\sigma} - \sigma'$ curves merged into a narrow band and α_P was estimated as 1.02, 1.02, and 1.06, for the Boise, Berea and Bandera sandstones, respectively. See Table 7 for details of these three sandstone experiments and also the Bakken shale.

Ling et al. [82] measured the $C_{b\sigma}$ and C_{bP} in nine samples of the Bakken shale and estimated C_s using Eq. (59); $\alpha_b$varied between 0.55 and 0.91 for all the samples.

Detailed experimental results from measuring the pore and bulk compressibilities, undrained compressibility, and unjacketed grain compressibility for the Penrith, Doddington, and Stainton sandstones are provided in Ref. [102].

5 Discussion of Factors Affecting the Effective Stress Coefficient

5.1 Effect of Porosity and Pore Shape. The higher the porosity, the lower will be the bulk modulus of the porous rock; consequently, the Biot coefficient will be higher. Wu [134] found a correlation between the Biot coefficient of a sandstone (measured using a static method) and porosity; the Biot coefficient increased with an increase in porosity. Reference [105] measured a higher Biot coefficient for samples of the Fontainebleau sandstone having $Ø = 9\%$ compared with samples with $Ø = 4\%$, at different simple effective stresses up to 100 MPa. The paper [135] also reported that the Biot coefficient of argillaceous rocks increases as the porosity increases. However, a recent attempt [81] was unsuccessful in finding any clear correlation between the Biot coefficients of the Bakken shale and the porosity or permeability of the rock.

The main question to be considered is: Why are α and effective stress coefficients in general large even in low-porosity rocks, as observed so far in this article? Biot's theory of poroelasticiy considers the elastic behavior of a porous medium at a macroscopic level [93]; thus, Biot's effective stress coefficient as defined in Eq. (15) is independent of the pore shape. However, it was shown by succeeding studies that the bulk modulus (or compressibility) of a rock depends not only on the porosity but also on the pore geometry. According to [136], microcracks and joints in a rock sample increase their compressibility (or decrease K). Reference [137] found that the compressibility theoretically depends on the parameter $\frac{hA_{\text{crack}}}{V}$, where h represents the standard deviation of the asperity heights and $\frac{A_{\text{crack}}}{V}$ is the total area of the cracks per unit volume of the rock. Using the effective medium theory, the key parameters affecting compressibility (or bulk modulus) of an elastic solid containing many cracks are the crack density defined as $\frac{\text{Na}^3}{V}$, where N is number of the cracks with a dimension a, the crack aspect ratio, and the porosity [137–140].

Given that the grain modulus is independent of the pore shape but the bulk modulus does decrease with an increase in the crack density, it can be concluded that Biot's effective stress coefficient is also dependent on the pore geometry. Reference [140] analytically showed that the Biot coefficient of an elastic porous medium is dependent on the shape of the pores and the crack density; the Biot coefficient increases with an increase in the crack density.

It was also demonstrated [141] that there exist direct correlations between the Biot coefficients of various sedimentary and crystalline rocks and the pore throat apertures. Based on this linear function, α increased with an increase in the pore throat aperture.

A two-dimensional (2D) numerical study of a hard rock [142] demonstrated that elongated pores and cracks significantly increase α compared to circular pores, even if the porosities remain the same. They related this phenomenon to the fact that elongated pores and cracks have significantly smaller shape factors S as defined by

$$S = \frac{4\pi A}{L_1^2} \tag{68}$$

where A is the total area of the pores and cracks and L_1 is the pore perimeter in a 2D case.

Reference [142] also numerically proved that elongated pores and cracks and their orientations to the loading direction create an anisotropic response for the Biot coefficient, resulting in a greater α normal to the crack axis. Tan et al. [143] conducted 2D discrete element modeling of a triaxial test on an Aue granite sample with an initial porosity of 2.3% under confining stress and pore pressure of 20 MPa and 10 MPa, respectively, and studied the Biot coefficient evolution during failure. Their numerical results revealed that α approximately follows a piecewise function; α is nearly constant below the crack initiation stress, it linearly increases to approximate unity at the crack damage stress, and remains constant thereafter.

For higher porosity media such as soils, it can be concluded that $\alpha = 1$, as in Terzaghi's effective stress principle, is related to the large volume of the pores and cracks, not the porosity itself.

Detailed discussions regarding the effective stress coefficient of fractured rocks can be found elsewhere [144,145].

5.2 Effect of Simple Effective Stress. A porous rock usually exhibits a nonlinear behavior, its jacketed bulk modulus increases with an increase in simple or Terzaghi's effective stress (see Fig. 3). As a result, the effective stress coefficient decreases with an increase in Terzaghi's effective stress [62,63,79,105,122,146–148]; however, the Biot theory still holds if applied over incremental stress variations.

5.3 Effect of Stress Anisotropy. Although Eq. (9) was originally developed for the isotropic compression condition, a few studies have also measured the Biot coefficient under anisotropic stress conditions.

In Ref. [85] an attempt was made to estimate the Biot coefficient of saturated Kansas chalk samples following isotropic-isochoric compression tests. The confining stress was varied to maintain only a constant axial strain (and not a volumetric strain) in the sample, by increasing the pore pressure (see Table 3); the authors claimed that the measured lateral strain was negligible.

Reference [65] measured α of the Berea sandstone utilizing the jacketed-unjacketed test and the bulk-pore volume changes technique in a plane-strain triaxial apparatus that applied anisotropic stress conditions on the sample (Table 2).

One could expect a different Biot coefficient from an anisotropic stress condition compared to the isotropic test, which could be due to the potential to develop localized shear strain in the rock.

5.4 Effect of Loading–Unloading Cycles. Some of the cases reviewed in this work involved seasoning or preconditioning the samples by several loading-unloading cycles before testing. In other cases, the actual techniques used for measuring the effective stress coefficient involved loading-unloading patterns. The loading-unloading can induce irreversible deformation of the porous skeleton. Both the one-dimensional and three-dimensional linear theories of consolidation proposed by Terzaghi [52] and Biot [1], respectively, have limitations as they do not account for the irreversibility of the skeletal deformations when elastoplastic unloading is involved. This issue is beyond the scope of this review and was highlighted in a recent study by Ref. [55].

Bernabé et al. [120] reported that the effect of the loading history becomes less significant once the sample has undergone a few (preconditioning) loading-unloading cycles before the test. They made this claim based on the effect of hysteresis and inelasticity of the rock on the permeability results.

Reference [112] reported a greater permeability effective stress coefficient during unloading than loading of the Pottsville sandstone and Pigeon Cove granite.

The authors of Ref. [115] did not observe any significant changes in the permeability effective stress coefficient for the Westerly granite as a result of three loading-unloading cycles ($\sigma = 10 - 96\,\text{MPa}$, $P = 1 - 86$ MPa) where the effective stress coefficients were determined to be 0.95–1.23 (Table 4).

5.5 Effect of Material Anisotropy. In isotropic poroelastic media, the Biot coefficient takes a scalar form; however, many scholars discussed that α in transversely isotropic media such as argillaceous formations including shales and mudstones, can be defined as a tensor. The extension of the isotropic theory of linear poroelasticity to a porous anisotropic solid was originally undertaken by Biot [149]. Additional theoretical developments and some experimental results for the cases of anisotropic poroelasticity have been provided by many researchers (e.g., Refs. [6,69,76], and [150–157]).

In measuring α for Bakken shale samples under isotropic stress conditions, Ref. [81] found that α was larger for the samples taken parallel to the bedding plane (average = 0.67) than for the samples collected normal to the bedding plane (average = 0.61).

For the two samples of Callovo–Oxfordian claystone, Belmokhtar et al. [69] measured different values for α in the directions perpendicular and parallel to the bedding plane using undrained and drained compressions of the claystone. The volumetric Biot coefficients were 0.85 and 0.90 for one sample and 0.87 and 0.98 for another sample, perpendicular and parallel to the bedding plane, respectively. The anisotropic Biot coefficients showed greater variations compared to the volumetric α which is 0.87–0.91 (Table 1).

Hu et al. [71] determined Biot coefficients equal to 0.99 and 0.97 for the Opalinus clay in the directions perpendicular and parallel to the bedding plane, respectively. These values are slightly greater than the volumetric Biot coefficient of the Opalinus clay, which is 0.95 (Table 1).

Theoretical developments and experimental studies to measure the effective stress coefficient for a vertically transverse isotropic (VTI) rock such as coal are discussed in Ref. [154].

In Ref. [135] the Biot coefficients were estimated in different directions to the bedding plane using the in situ specific storage coefficient of argillaceous rocks.

For the Chelmsford granite, Ref. [112] tested samples from different orientations but did not observe any significant difference in the permeability effective stress coefficient for the different samples.

5.6 Effect of Measurement Technique. Various techniques applied to the same sample can yield different results for the effective stress coefficient; Ref. [69] reported slight differences in the Biot coefficient of the Callovo–Oxfordian claystone; using the jacketed-unjacketed test method resulted in $\alpha = 0.85$ while estimating the Biot coefficient based on other poroelastic parameters using Eq. (33) yielded $\alpha = 0.91$.

da Silva et al. [72] determined $\alpha = 0.84$ for samples of the Sorcy limestone using the jacketed–unjacketed test technique whereas the bulk-pore volume changes and estimation from other poroelastic parameters (Eq. (33)) resulted in Biot coefficients of 0.81 and 0.85, respectively.

Figure 12 shows how the two methods based on isotopic stress conditions (i.e., jacketed–unjacketed test method, matching volumetric strain of dry, and saturated samples) resulted in slightly different values for α for the entire range of the applied effective stresses. The failure envelope method was expected to yield higher values for the effective stress coefficient but surprisingly it was close to the results produced using the matching volumetric strain method.

Another observation from Fig. 12 is that the effective stress coefficient decreased as the effective stress increased. This is affirmation of the discussion given in Sec. 5.2.

5.7 Effect of Test Temperature. The theory of linear poroelasticity has been extended to nonisothermal conditions and a complete presentation of the analytical equations can be found, for example, in Ref. [76]. The Biot coefficient is influenced by the test temperature; the effect is dependent on how the two parameters (i.e., the drained bulk modulus and the unjacketed bulk modulus) in Eq. (15) are affected by the temperature. In a drained condition, where Terzaghi's effective stress is maintained constant, any alterations in the bulk modulus are the result of thermal

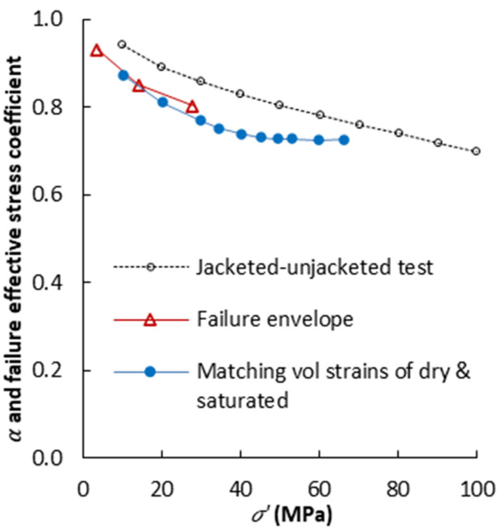

Fig. 12 Biot coefficient and failure state effective stress coefficient of a sandstone (data from Ref. [87])

expansion of the porous skeleton [76]. Grain bulk moduli of rock minerals are also dependent on the thermal softening of the minerals.

Reference [62] determined α for the Flechtinger sandstone following Eq. (15). The test scheme included loading-unloading between 2 MPa and 55 MPa at each temperature. No remarkable changes were observed in α determined from the jacketed-unjacketed test with respect to test temperature. However, Ref. [62] reported that α calculated using the bulk and pore volume change method was 0.76–1 at 30 °C (under different simple effective stresses) whereas it reduced to between 0.54 and 0.94 at 140 °C (Fig. 13). Overall, the experiments by Ref. [61] contained the combined effects of loading-unloading and temperature (Fig. 13). Studying only the temperature effects (and not loading-unloading cycles) would require a dedicated test under constant σ and P but varying temperatures.

In another publication [158], a reverse trend to that shown in Fig. 13 was observed for the Biot coefficients of the Malm

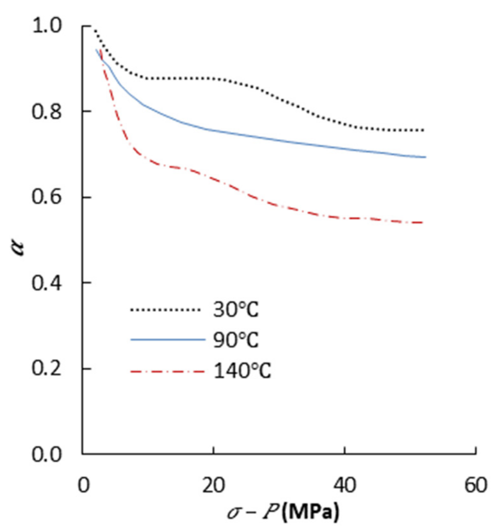

Fig. 13 Biot coefficient of the Flechtinger sandstone at different temperatures during loading path $\sigma = 2$ to 55 MPa under pore pressure $P = 1$ MPa as a function of Terzaghi's effective stress. The bulk-pore volume change technique was used (data from Ref. [62]). The results contain the combined effects of loading-unloading cycles and temperature.

carbonate determined using the jacketed-unjacketed test method. The values of α were found to be slightly higher at 60 °C than at 30 °C at all Terzaghi's effective stresses in the range of about 3–72 MPa. It is not clear to the authors of this review paper how the test results were affected by the preconditioning of the sample, which included raising the sample temperature to 60 °C under unconfined conditions followed by several cycles of loading-unloading with a confining stress between 0 and 80 MPa.

The jacketed-unjacketed test results of the Indo-Chinese granodiorite (Table 1) showed that at low Terzaghi's effective stresses, the Biot coefficient increased as the test temperature increased; however, a reverse effect was observed at higher effective stresses [68].

Studying the effective stress coefficient of organic rocks, such as coal, which undergo structural changes at high temperatures due to the chemical process of pyrolysis (e.g., Ref. [159]) is beyond the scope of this review.

5.8 Effect of Pore Fluid Type. The Biot coefficient is theoretically independent of the pore fluid type. The cases reviewed in this article used water, de-ionized water, distilled water, butane, and inert gases such as nitrogen or argon, as pore fluids. Using an inert gas alleviates any chemical interactions with clay minerals within the rock sample as well as the capillary effects that may exist when using water as the pore fluid. However, if the effective stress coefficient is determined via permeability measurements at low pore pressures, the gas slippage effect (see Ref. [160]) must be accounted for in order not to adversely affect the determination of the effective stress coefficient.

5.9 Effect of Sample Size. The case studies reviewed here used samples that varied in diameter from 19 mm to 60 mm and in length from 10 mm to 125 mm. One exception was the test conducted by Ref. [53] that measured the bulk modulus of the Cobourg limestone from a sample 150 mm in diameter and 300 mm long, which was chosen due to the heterogeneity of the limestone. The dimensions of a testing specimen should be selected such that it can be regarded as the representative elementary volume of the rock under study.

5.10 Effect of Clay Content. Some studies suggested that the Biot and other effective stress coefficients of clay-bearing rocks are dependent on the clay content; the higher the clay content, the higher is the effective stress coefficients [161,162]. In studying unjacketed grain compressibilities of three sandstones with different clay contents, [102] observed that the rock with the higher clay content showed greater compressibility.

5.11 Effective Stress Coefficient Greater Than Unity. Based on Eq. (15), α cannot be greater than unity. However, some of the cases reported effective stress coefficients greater than unity; where the testing techniques were based on partial derivatives of permeability, deformation, or geophysical properties with respect to pore pressure and confining stress (or simple effective stress) (e.g., see Tables 4–7). Other studies also reported permeability effective stress coefficients greater than one (e.g., Ref. [26]). Reference [102] even reported a value of 5.4 for the effective stress coefficient of the Stainton sandstones based on the changes in permeability caused by variations in the confining stress and pore pressure. The testing conditions that resulted in effective stress coefficients greater than unity involved inelastic loading states and, therefore, do not follow the upper limit of for Biot coefficient (i.e., $\alpha \leq 1.0$) which was derived based on the theory of linear poroelasticity.

5.12 Accuracy in Reporting the Effective Stress Coefficient. Throughout this review, Biot and other effective stress coefficients have been reported to the accuracy provided in the references cited; however, they have been rounded up by the authors of this review to no more than two decimal places.

Generally, the accuracy in reporting Biot and other effective stress coefficients and the recommended significant digits is dependent on the number of decimal places involved in determining the parameters needed for calculating the coefficient, which should follow available standards or best practices in each discipline. For example, recording geotechnical data (such as water content, porosity, stress, and elastic moduli) can follow [163]; however, this standard does not have any recommendation for number of decimal places or significant digits for the Biot and other effective stress coefficients. Overall, the suggested number of decimal places in reporting Biot and other effective stress coefficients is outside the focus of this review.

5.13 Effective Stress Coefficient for Numerical Modeling. As demonstrated in this review, the effective stress coefficient is a state parameter. The effective stress coefficient cannot be constant; it is dependent on several factors (i.e., mean effective stress, temperature, and material state with respect to failure) that can be associated with a material point in the modeling. Ideally, the effective stress coefficient needs to be assigned to different grid points of an HM or a THM model as a function of the aforementioned factors, if such constitutive relations are available from laboratory or in situ experiments.

6 Concluding Remarks

This study reviewed the approaches that have been proposed in the literature to measure the Biot coefficient and other effective stress coefficients of fluid-saturated rocks. Several case studies were reported for each method. The following observations can be drawn based on this review:

- The effective stress coefficient can be determined for different conditions, such as isotropic poroelasticity (i.e., Biot coefficient), inelasticity, or failure states.
- The original technique for determining the Biot coefficient was introduced for rocks with an elastic porous skeleton under isotropic stress conditions.
- The bulk-pore volume changes and isotropic-isochoric compression were both analytically derived from the original technique; hence, they provide the Biot coefficient for the elastic condition as well.
- The method based on matching the volumetric strain of dry and saturated samples was also proposed for the elastic state under isotropic compression, and thus, represents the Biot coefficient for the elastic condition.
- Other methods, which are based on partial derivatives of permeability, axial or volumetric deformation, and geophysical properties with respect to pore pressure and confining stress (or simple effective stress), usually involve loading-unloading cycles as part of the testing procedures. Therefore, it can be concluded that these methods suffer from potential irrecoverable deformation of the rock if broad ranges of confining stresses and/or pore pressures are applied to the sample. The resulting effective stress coefficients are different from the Biot coefficient which is only applicable to isotropic linear poroelasticity.
- The failure envelope method provides the effective stress coefficient for failure or residual strength conditions, which can be different from elastic compression under isotropic stress conditions.
- The bulk modulus estimated from geophysical measurements can differ from the static techniques due to the difference in strain amplitudes. Moreover, at ultrasonic frequencies, following the application of an external load on a saturated rock, the fluid pressure can be different from pore to pore; consequently, there is a lack of local fluid pressure equilibrium. These conditions invalidate the conditions of the theory of poroelasticity. As a result, the effective stress coefficients are different from the Biot coefficient.
- The effective stress coefficients in hard crystalline rocks are affected by the presence of elongated pores and cracks. The Biot coefficient is independent of the pore geometry; however, it was later demonstrated that the bulk compressibility is a function of pore shape, crack aspect ratio, and crack density. As a result, the Biot coefficient is a function of the pore geometry.
- Increasing simple effective stress will result in a reduction in the effective stress coefficient.
- In weak argillaceous rocks, α measured at different orientations to the bedding plane can be different.
- Other factors that influence the effective stress coefficient are the stress path and test temperature.

Acknowledgment

The support provided by the Nuclear Waste Management Organization (NWMO), Toronto, Canada to the lead author in preparation of the paper is greatly acknowledged. Both authors are thankful to Dr. Monique Hobbs and Dr. Paul Gierszewski of the NWMO and the anonymous reviewers of this journal for their critical reviews of the paper. The editorial assistance provided by Mrs. S. J. Selvadurai is gratefully acknowledged.

Author Contributions

HAK prepared the initial and subsequent versions of the paper. APSS contributed to the conceptual and editorial changes to several versions of the article.

Nomenclature

a = crack dimension
A = total area of pores and cracks
A_{crack} = total area of the cracks
B = Skempton's pore pressure coefficient
c = cohesion
C_b = jacketed compressibility
C_{bP} = bulk compressibility induced by variations of pore pressure
$C_{b\sigma}$ = bulk compressibility induced by variations of confining stress
C_{PP} = pore compressibility caused by changes in pore pressure
$C_{P\sigma}$ = pore compressibility caused by changes in confining stress
C_s = unjacketed compressibility
D = cylindrical sample diameter
dW = work increment for an isotropic stress state
E = Young's modulus
E_{oed} = oedometric modulus
E_x = Young's modulus in the direction parallel to the bedding plane
E_z = Young's modulus in the direction perpendicular to the bedding plane
P = pore pressure
G = shear modulus of the drained elastic solid
h = standard deviation of the asperity heights
H = a physical constant
H' = a physical constant
k = permeability
K = bulk modulus of the drained elastic solid or jacketed bulk modulus
k^{λ} = transformed permeability
K_s = unjacketed bulk modulus
K_u = undrained bulk modulus
K'_s = bulk modulus of minerals
L = cylindrical sample length
L_1 = pore perimeter in a 2D case

N = number of cracks
q = a property of rock such as permeability
Q = a physical constant
Q_P = attenuation factor
R = a physical constant
R_1 = a physical constant
s = storage coefficient
S = shape factor
UCS = unconfined compressive strength
V = bulk volume
V_b = bulk volume
V_p = pore fluid volume
$V_{P\text{wave}}$ = compressional wave velocity
$V_{S\text{wave}}$ = shear wave velocity
α = Biot's coefficient
α_b = Biot's coefficient deduced from bulk compressibility values induced by variations of pore pressure confining stress
α_f = effective stress coefficient for failure state
α_k = effective stress coefficient from variations of permeability
$\alpha_{k.\text{cubic}}$ = effective stress coefficient for permeability from cubic root equation
$\alpha_{k.\text{der}.P\&\sigma}$ = effective stress coefficient from partial derivatives of permeability with respect to pore pressure and confining stress
$\alpha_{k.\text{tran}.P\&\sigma}$ = effective stress coefficient from response surface and variations of transformed permeability
$\alpha_{k.\text{trial}}$ = effective stress coefficient from trial-and-error method in curve fitting to permeability data
α_{oed} = Biot's coefficient under oedometric conditions
α_P = Biot's coefficient deduced from pore compressibility values induced by variations of pore pressure confining stress
$\alpha_{q.\text{der}.P\&\sigma}$ = effective stress coefficient from partial derivatives of parameter q with respect to pore pressure and confining stress
$\alpha_{q.\text{der}.P\&\sigma'_s}$ = effective stress coefficient from partial derivatives of parameter q with respect to pore pressure and simple effective stress
$\alpha_{Q.\text{der}.P\&\sigma'_s}$ = effective stress coefficient from partial derivatives of attenuation factor with respect to pore pressure and simple effective stress
$\alpha_{V_{P\text{wave}}.\text{der}.P\&\sigma'_s}$ = effective stress coefficient from partial derivatives of compressional wave velocity with respect to pore pressure and simple effective stress
$\alpha_{V_{S\text{wave}}.\text{der}.P\&\sigma'_s}$ = effective stress coefficient from partial derivatives of shear wave velocity with respect to pore pressure and simple effective stress
$a_1, \ldots, a_6$ = coefficients of quadratic regression analysis
$\alpha_{\varepsilon.P\&\sigma'_s}$ = effective stress coefficient from partial derivatives of strain with respect to pore pressure and simple effective stress
$\alpha_{\varepsilon_a.\text{der}.P\&\sigma'_s}$ = effective stress coefficient from partial derivatives of ε_a with respect to pore pressure and simple effective stress
$\alpha_{\varepsilon_v.\text{der}.P\&\sigma'_s}$ = effective stress coefficient from partial derivatives of ε_v with respect to pore pressure and simple effective stress
$\alpha_{\varepsilon_v.\text{tran}.P\&\sigma}$ = effective stress coefficient from response surface and variations of transformed volumetric strain
δ_{ij} = Kronecker delta
ε_a = axial strain
ε_{ij} = small strain tensor
ε_r = radial strain
ε_v = volumetric strain
ε_v^λ = transformed volumetric strain
ν_{xy} = Poisson's ratios in the direction parallel to the bedding plane
ν_{zx} = Poisson's ratios in the direction perpendicular to the bedding plane
ρ_{dry} = dry bulk density
σ_{ij} = total stress or total isotropic confining stress tensor
σ'_{ij} = Biot's effective stress tensor
σ'_s = simple effective stress or Terzaghi's effective stress
σ_1 = maximum principal stress
σ_3 = minimum principal stress
Ø = porosity
λ = Lame's parameter under drained condition
ν = Poisson's ratio
ξ = variation of fluid content
φ = friction angle
ψ = slope of the failure envelope in the $\sigma'_1 - \sigma'_3$ plane

References

[1] Biot, M. A., 1941, "General Theory of Three-Dimensional Consolidation," J. Appl. Phys., **12**(2), pp. 155–164.
[2] Biot, M. A., and Willis, D. G., 1957, "The Elastic Coefficients of the Theory of Consolidation," ASME J. Appl. Mech., **24**(4), pp. 594–601.
[3] Fan, X., Li, G., Shah, S. N., Tian, S., Sheng, M., and Geng, L., 2015, "Analysis of a Fully Coupled Gas Flow and Deformation Process in Fractured Shale Gas Reservoirs," J. Nat. Gas Sci. Eng., **27**, pp. 901–913.
[4] Jin, L., and Zoback, M., 2019, "Depletion-Induced Poroelastic Stress Changes in Naturally Fractured Unconventional Reservoirs and Implications for Hydraulic Fracture Propagation," SPE Annual Technical Conference and Exhibition, Society of Petroleum Engineers, Calgary, AB, Canada, Sept. 30–Oct. 2, Paper No. SPE-196215-MS.
[5] Segall, P., Grasso, J. R., and Mossop, A., 1994, "Poroelastic Stressing and Induced Seismicity Near the Lacq Gas Field, Southwestern France," J. Geophys. Res. Solid Earth, **99**(B8), pp. 15423–15438.
[6] Bui, B., and Tutuncu, A., 2013, "Biot Tensor Approach for Improved Lifecycle Well Integrity," Proceedings of 47th U.S. Rock Mechanics/Geomechanics Symposium, American Rock Mechanics Association, San Francisco, CA, June 23–26, Paper No. ARMA-2013341.
[7] Selvadurai, A., P. S., Zhang, D., and Kang, Y., 2018, "Permeability Evolution in Natural Fractures and Their Potential Influence on Loss of Productivity in Ultra-Deep Gas Reservoirs of the Tarim Basin, China," J. Nat. Gas Sci. Eng., **58**, pp. 162–177.
[8] Zhang, D., Kang, Y., Selvadurai, A. P. S., and You, L., 2020, "Experimental Investigation of the Effect of Salt Precipitation on the Physical and Mechanical Properties of a Tight Sandstone," Rock Mech. Rock Eng., **53**(10), pp. 4367–4380.
[9] Azeemuddin, M., Khan, K., Khan, M. N., Abdulraheem, A., Rahim, Z., and Al-Qahtani, M. Y., 2002, "Experimental Determination of Elastic Anisotropy and Biot's Constant in a Saudi Arabian Reservoir Sandstone," Proceedings of Abu Dhabi International Petroleum Exhibition and Conference, Society of Petroleum Engineers, Abu Dhabi, UAE, Oct. 13–16, Paper No. SPE-78503-MS.
[10] Kasani, H. A., and Chalaturnyk, R. J., 2017, "Coupled Reservoir and Geomechanical Simulation for a Deep Underground Coal Gasification Project," J. Nat. Gas Sci. Eng., **37**, pp. 487–501.
[11] Rutqvist, J., and Tsang, C. F., 2005, "Coupled Hydromechanical Effects of CO_2 Injection," Dev. Water Sci., **52**, pp. 649–679.
[12] Vilarrasa, V., Olivella, S., and Carrera, J., 2011, "Geomechanical Stability of the Caprock During CO_2 Sequestration in Deep Saline Aquifers," Energy Procedia, **4**, pp. 5306–5313.
[13] Haimson, B., and Fairhurst, C., 1969, "Hydraulic Fracturing in Porous-Permeable Materials," J. Pet. Technol., **21**(07), pp. 811–817.
[14] Li, S., Li, X., and Zhang, D., 2016, "A Fully Coupled Thermo-Hydro-Mechanical, Three-Dimensional Model for Hydraulic Stimulation Treatments," J. Nat. Gas Sci. Eng., **34**, pp. 64–84.
[15] Kohl, T., Evansi, K. F., Hopkirk, R. J., and Rybach, L., 1995, "Coupled Hydraulic, Thermal and Mechanical Considerations for the Simulation of Hot Dry Rock Reservoirs," Geothermics, **24**(3), pp. 345–359.
[16] Wessling, S., Junker, R., Rutqvist, J., Silin, D., Sulzbacher, H., Tischner, T., and Tsang, C. F., 2009, "Pressure Analysis of the Hydromechanical Fracture Behaviour in Stimulated Tight Sedimentary Geothermal Reservoirs," Geothermics, **38**(2), pp. 211–226.
[17] Mouli-Castillo, J., Wilkinson, M., Mignard, D., McDermott, C., Haszeldine, R. S., and Shipton, Z. K., 2019, "Inter-Seasonal Compressed-Air Energy Storage Using Saline Aquifers," Nat. Energy, **4**(2), pp. 131–139.
[18] Sánchez, M., Shastri, A., and Le, T. M., 2014, "Coupled Hydromechanical Analysis of an Underground Compressed Air Energy Storage Facility in Sandstone," Geotech. Lett., **4**(2), pp. 157–164.
[19] Guo, R., Xu, H., Plúa, C., and Armand, G., 2020, "Prediction of the Thermal-Hydraulic-Mechanical Response of a Geological Repository at Large Scale and Sensitivity Analyses," Int. J. Rock Mech. Min. Sci., **136**, p. 104484.
[20] Guo, R., Thatcher, K. E., Seyedi, D. M., and Plúa, C., 2020, "Calibration of the Thermo-Hydro-Mechanical Parameters of the Callovo-Oxfordian Claystone and the Modelling of the ALC Experiment," Int. J. Rock Mech. Min. Sci., **132**, p. 104351.

[21] Nguyen, T. S., and Selvadurai, A. P. S., 1995, "Coupled Thermal-Mechanical-Hydrological Behaviour of Sparsely Fractured Rock: Implications for Nuclear Fuel Waste Disposal," Int. J. Rock Mech. Min. Sci., **32**(5), pp. 465–479.
[22] Radakovic-Guzina, Z., and Damjanac, B., 2019, "Sensitivity Analyses of Long-Term Stability of APM Conceptual Repository Designs in Crystalline and Sedimentary Rock Settings," Itasca Consulting Group, Report for Nuclear Waste Management Organization (NWMO), Minneapolis, MN, Report No. NWMO-TR-2019-08.
[23] Barbour, A. J., Xue, L., Roeloffs, E., and Rubinstein, J. L., 2019, "Leakage and Increasing Fluid Pressure Detected in Oklahoma's Wastewater Disposal Reservoir," J. Geophys. Res. Solid Earth, **124**(3), pp. 2896–2919.
[24] Zhai, G., Shirzaei, M., and Manga, M., 2020, "Elevated Seismic Hazard in Kansas Due to High-Volume Injections in Oklahoma," Geophys. Res. Lett., **47**(5), p. e2019GL085705.
[25] Chen, Y., Selvadurai, A. P. S., and Liang, W., 2019, "Computational Modelling of Groundwater Inflow During a Longwall Coal Mining Advance: A Case Study From the Shanxi Province, China," Rock Mech. Rock Eng., **52**(3), pp. 917–934.
[26] Li, X., Feng, Y., El Mohtar, C. S., and Gray, K. E., 2019, "Transient Modeling of Borehole Breakouts: A Coupled Thermo-Hydro-Mechanical Approach," J. Pet. Sci. Eng., **172**, pp. 1014–1024.
[27] Roshan, H., and Rahman, S. S., 2011, "Analysis of Pore Pressure and Stress Distribution Around a Wellbore Drilled in Chemically Active Elastoplastic Formations," Rock Mech. Rock Eng., **44**(5), pp. 541–552.
[28] Kim, J., and Selvadurai, A. P. S., 2015, "Ground Heave Due to Line Injection Sources," Geomech. Energy Environ., **2**, pp. 1–14.
[29] Schwartzkopff, A. K., Sainoki, A., and Elsworth, D., 2021, "Numerical Simulation of an in-Situ Fluid Injection Experiment Into a Fault Using Coupled X-FEM Analysis," Rock Mech. Rock Eng., **54**(3), pp. 1027–1053.
[30] Neuzil, C. E., 2003, "Hydromechanical Coupling in Geologic Processes," Hydrogeol. J., **11**(1), pp. 41–83.
[31] Van der Kamp, G., and Gale, J. E., 1983, "Theory of Earth Tide and Barometric Effects in Porous Formations With Compressible Grains," Water Resour. Res., **19**(2), pp. 538–544.
[32] Selvadurai, A. P. S., Suvorov, A. P., and Selvadurai, P. A., 2015, "Thermo-Hydro-Mechanical Processes in Fractured Rock Formations During a Glacial Advance," Geosci. Model Dev., **8**(7), pp. 2167–2185.
[33] Cheng, A. H. D., 2016, *Poroelasticity*, Vol. 877, Springer International Publishing, Switzerland.
[34] Selvadurai, A. P. S., and Suvorov, A. P., 2017, *Thermo-Poroelasticity and Geomechanics*, Cambridge University Press, Cambridge, UK.
[35] Carcione, J. M., 2015, "Wave Fields in Real Media: Wave Propagation in Anisotropic," *Anelastic, Porous and Electromagnetic Media*, 3rd ed., Elsevier, Amsterdam, The Netherlands.
[36] Lee, M. W., 2006, "Explicit Use of the Biot Coefficient in Predicting Shear-Wave Velocity of Water-Saturated Sediments," Geophys. Prospect., **54**(2), pp. 177–185.
[37] Selvadurai, A. P. S., and Najari, M., 2017, "The Thermo-Hydro-Mechanical Behavior of the Argillaceous Cobourg Limestone," J. Geophys. Res. Solid Earth, **122**(6), pp. 4157–4171.
[38] Selvadurai, A. P. S., and Najari, M., 2013, "On the Interpretation of Hydraulic Pulse Tests on Rock Specimens," Adv. Water Resour., **53**, pp. 139–149.
[39] Selvadurai, A. P. S., and Suvorov, A. P., 2014, "Thermo-Poromechanics of a Fluid-Filled Cavity in a Fluid-Saturated Geomaterial," Proc. Math. Phys. Eng. Sci., **470**(2163), p. 20130634.
[40] Schrefler, B. A., 2002, "Mechanics and Thermodynamics of Saturated/Unsaturated Porous Materials and Quantitative Solutions," ASME Appl. Mech. Rev., **55**(4), pp. 351–388.
[41] Steeb, H., and Renner, J., 2019, "Mechanics of Poro-Elastic Media: A Review With Emphasis on Foundational State Variables," Transp. Porous Media, **130**(2), pp. 437–461.
[42] Selvadurai, A. P. S., 2007, "The Analytical Method in Geomechanics," ASME Appl. Mech. Rev., **60**(3), pp. 87–106.
[43] Rudnicki, J. W., 2001, "Coupled Deformation-Diffusion Effects in the Mechanics of Faulting and Failure of Geomaterials," ASME Appl. Mech. Rev., **54**(6), pp. 483–502.
[44] Kasani, H. A., 2019, "Current Laboratory Techniques for Measuring Biot's Coefficient of Rock: A Review," Proceedings of 14th International Congress on Rock Mechanics and Rock Engineering (ISRM 2019), da Fontoura et al., eds., Foz do Iguassu, Brazil, Sept. 13–18, Paper No. ISRM-14CONGRESS-2019-181.
[45] Cariou, S., Duan, Z., Davy, C., Skoczylas, F., and Dormieux, L., 2012, "Poromechanics of Partially Saturated COx Argillite," Appl. Clay Sci., **56**, pp. 36–47.
[46] Vlahinić, I., Jennings, H. M., Andrade, J. E., and Thomas, J. J., 2011, "A Novel and General Form of Effective Stress in a Partially Saturated Porous Material: The Influence of Microstructure," Mech. Mater., **43**(1), pp. 25–35.
[47] Yuan, H., Agostini, F., Duan, Z., Skoczylas, F., and Talandier, J., 2017, "Measurement of Biot's Coefficient for CO_x Argillite Using Gas Pressure Technique," Int. J. Rock Mech. Min. Sci., **92**, pp. 72–80.
[48] Suvorov, A. P., and Selvadurai, A. P. S., 2019, "The Biot Coefficient for an Elasto-Plastic Material," Int. J. Eng. Sci., **145**, p. 103166.
[49] Detournay, ECheng,., and A. H. D., 1993, "Fundamentals of Poroelasticity," *Comprehensive Rock Engineering: Principles, Practice and Projects* (In Analysis and Design Methods), Vol. II, C. Fairhurst, ed., Pergamon Press, Oxford, UK, pp. 113–171.
[50] Wang, H. F., 2000, *Theory of Poroelasticity With Applications to Geomechanics and Hydrogeology*, Princeton University Press, Princeton, NJ.
[51] Cowin, S. C., and Benalla, M., 2011, "Graphical Illustrations for the Nur-Byerlee-Carroll Proof of the Formula for the Biot Effective Stress Coefficient in Poroelasticity," J. Elast., **104**(1–2), pp. 133–141.
[52] Terzaghi, K., 1923, "Die Berechnung Der Durchlassigkeitsziffer Des Tones Aus Dem Verlauf Der Hydrodynamischen Spannungserscheinungen," Akad. Wiss. Wien Sitzungsber. Mathnaturwissensch. Klasse IIa, **142**, pp. 125–138.
[53] Selvadurai, A. P. S., 2019, "The Biot Coefficient for a Low Permeability Heterogeneous Limestone," Contin. Mech. Thermodyn., **31**(4), pp. 939–953.
[54] Selvadurai, A. P. S., 2019, "A Multi-Phasic Perspective of the Intact Permeability of the Heterogeneous Argillaceous Cobourg Limestone," Sci. Rep., **9**(1), pp. 17388.
[55] Selvadurai, A. P. S., 2021, "Irreversibility of Soil Skeletal Deformations: The Pedagogical Limitations of Terzaghi's Celebrated Model for Soil Consolidation," Comput. Geotech., **135**, p. 104137.
[56] Rice, J. R., and Cleary, M. P., 1976, "Some Basic Stress Diffusion Solutions for Fluid-Saturated Elastic Porous Media With Compressible Constituents," Rev. Geophys., **14**(2), pp. 227–241.
[57] Nur, A., and Byerlee, J., 1971, "An Exact Effective Stress Law for Elastic Deformation of Rock With Fluids," J. Geophys. Res., **76**(26), pp. 6414–6419.
[58] Berryman, J. G., 1992, "Effective Stress for Transport Properties of Inhomogeneous Porous Rock," J. Geophys. Res. Solid Earth, **97**(B12), pp. 17409–17424.
[59] Mavko, G., Mukerji, T., and Dvorkin, J., 2009, "The Rock Physics Handbook," *Tools for Seismic Analysis of Porous Media*, Cambridge University Press, Cambridge, UK.
[60] Selvadurai, A. P. S., Selvadurai, P. A., and Nejati, M., 2019, "A Multi-Phasic Approach for Estimating the Biot Coefficient for Grimsel Granite," Solid Earth, **10**(6), pp. 2001–2014.
[61] Selvadurai, A. P. S., 2021, "On the Poroelastic Biot Coefficient for a Granitic Rock," Geosciences, **11**(5), p. 219.
[62] Hassanzadegan, A., 2013, "Thermomechanical and Poromechanical Behavior of Flechtinger Sandstone," Ph.D. thesis, der Technischen Universitat, Berlin, Germany.
[63] Ingraham, M. D., Bauer, S. J., Issen, K. A., and Dewers, T. A., 2017, "Evolution of Permeability and Biot Coefficient at High Mean Stresses in High Porosity Sandstone," Int. J. Rock Mech. Min. Sci., **96**, pp. 1–10.
[64] Hu, C., Agostini, F., Skoczylas, F., and Egermann, P., 2018, "Effects of Gas Pressure on Failure and Deviatoric Stress on Permeability of Reservoir Rocks: Initial Studies on a Vosges Sandstone," Eur. J. Environ. Civ. Eng., **22**(8), pp. 1004–1022.
[65] Makhnenko, R. M., and Labuz, J. F., 2013, "Unjacketed Bulk Compressibility of Sandstone in Laboratory Experiments," Poromechanics V – Proceedings of Fifth Biot Conference on Poromechanics, Vienna, Austria, July 10–12, pp. 481–488.
[66] Makhnenko, R. Y., 2013, "Deformation of Fluid-Saturated Porous Rock," Ph.D. thesis, University of Minnesota, MN.
[67] Hart, D. J., 2000, "Laboratory Measurements of Poroelastic Constants and Flow Parameters and Some Associated Phenomena," Ph.D. thesis, University of Wisconsin-Madison, WI.
[68] Zhang, Y., Hao, S., Bai, L., Yu, Z., Zhang, J., and Fang, J., 2018, "Thermomechanical Behavior of Late Indo-Chinese Granodiorite Under High Temperature and Pressure," J. Eng., **2018**, pp. 1–15.
[69] Belmokhtar, M., Delage, P., Ghabezloo, S., Tang, A. M., Menaceur, H., and Conil, N., 2017, "Poroelasticity of the Callovo–Oxfordian Claystone," Rock Mech. Rock Eng., **50**(4), pp. 871–889.
[70] Braun, P., Ghabezloo, S., Delage, P., Sulem, J., and Conil, N., 2019, "Determination of Multiple Thermo-Hydro-Mechanical Rock Properties in a Single Transient Experiment: Application to Shales," Rock Mech. Rock Eng., **52**(7), pp. 2023–2038.
[71] Hu, H., Braun, P., Delage, P., and Ghabezloo, S., 2021, "Evaluation of Anisotropic Poroelastic Properties and Permeability of the Opalinus Clay Using a Single Transient Experiment," Acta Geotech., **16**(7), pp. 2131–2142.
[72] da Silva, M. R., Schroeder, C., and Verbrugge, J. C., 2010, "Poroelastic Behaviour of a Water-Saturated Limestone," Int. J. Rock Mech. Min. Sci., **47**(5), pp. 797–807.
[73] Kim, K., and Makhnenko, R. Y., 2020, "Coupling Between Poromechanical Behavior and Fluid Flow in Tight Rock," Transp. Porous Media, **135**(2), pp. 487–512.
[74] Lau, J. S. O., and Chandler, N. A., 2004, "Innovative Laboratory Testing," Int. J. Rock Mech. Min. Sci., **41**(8), pp. 1427–1445.
[75] Lau, J. S. O., Gorski, B., Conlon, B., and Anderson, T., 2001, "The Measurement of Thermoporoelastic Parameters of Granite Using a Triaxial Cell," Attachment to the Incorporation of Rock Pore Pressure in Repository Design and Excavation Stability Analysis, Ontario Power Generation, Nuclear Waste Management Division, Toronto, ON, Canada, Report No. 06819-REP-01200-10068-R00.
[76] Guéguen, Y., Dormieux, L., and Boutéca, M., 2004, "Fundamentals of Poromechanics," *Mechanics of Fluid-Saturated Rocks*, Y. Guéguen, M. Bouteca, eds., Elsevier, Amsterdam, The Netherlands, pp. 1–54.
[77] Kümpel, H. J., 1991, "Poroelasticity: Parameters Reviewed," Geophys. J. Int., **105**(3), pp. 783–799.
[78] Müller, T. M., and Sahay, P. N., 2016, "Biot Coefficient is Distinct From Effective Pressure Coefficient," Geophysics, **81**(4), pp. L27–L33.
[79] Pimienta, L., Fortin, J., and Guéguen, Y., 2017, "New Method for Measuring Compressibility and Poroelasticity Coefficients in Porous and Permeable Rocks," J. Geophys. Res. Solid Earth, **122**(4), pp. 2670–2689.
[80] Ferrari, A., Favero, V., and Laloui, L., 2016, "One-Dimensional Compression and Consolidation of Shales," Int. J. Rock Mech. Min. Sci., **88**, pp. 286–300.

[81] He, J., Rui, Z., and Ling, K., 2016, "A New Method to Determine Biot Coefficients of Bakken Samples," J. Nat. Gas Sci. Eng., **35**, pp. 259–264.
[82] Ling, K., He, J., Pei, P., Wang, S., and Ni, X., 2016, "Comparisons of Biot Coefficients of Bakken Core Samples Measured by Three Methods," Proceedings of 50th U.S. Rock Mechanics/Geomechanics Symposium, American Rock Mechanics Association, Houston, TX, June 26–29, Paper No. ARMA-2016-030.
[83] Al-Tahini, A. M., Abousleiman, Y. N., and Brumley, J. L., 2005, "Acoustic and Quasi-Static Laboratory Measurement and Calibration of the Pore Pressure Prediction Coefficient in the Poroelastic Theory," Proceedings of SPE Annual Technical Conference and Exhibition, Society of Petroleum Engineers, Dallas, TX, Oct. 9–12, Paper No. SPE 95825.
[84] Blöcher, G., Reinsch, T., Hassanzadegan, A., Milsch, H., and Zimmermann, G., 2014, "Direct and Indirect Laboratory Measurements of Poroelastic Properties of Two Consolidated Sandstones," Int. J. Rock Mech. Min. Sci., **67**, pp. 191–201.
[85] Nermoen, A., Korsnes, R., Christensen, H. F., Trads, N., Hiorth, A., and Madland, M. V., 2013, "Measuring the Biot Stress Coefficient and is Implications on the Effective Stress Estimate," Proceedings of 47th U.S. Rock Mechanics/Geomechanics Symposium, American Rock Mechanics Association, San Francisco, CA, June 23–26, Paper No. ARMA-2013-282.
[86] Salemi, H., Iglauer, S., Rezagholilou, A., and Sarmadivaleh, M., 2018, "Laboratory Measurement of Biot's Coefficient and Pore Pressure Influence on Poroelastic Rock Behaviour," APPEA J., **58**(1), pp. 182–189.
[87] Franquet, J. A., and Abass, H. H., 1999, "Experimental Evaluation of Biot's Poroelastic Parameter - Three Different Methods," Vail Rocks 1999, 37th U.S. Symposium on Rock Mechanics (USRMS), American Rock Mechanics, Vail, CO, June 7–9, Paper No. ARMA-99-0349.
[88] Hill, R., 1952, "The Elastic Behaviour of a Crystalline Aggregate," Proc. Phys. Soc., **65**(5), pp. 349–354.
[89] Hashin, Z., and Shtrikman, S., 1963, "A Variational Approach to the Elastic Behavior of Multiphase Minerals," J. Mech. Phys. Solids, **11**(2), pp. 127–140.
[90] Reuss, A., 1929, "Berechnung Der Fließgrenze Von Mischkristallen Auf Grund Der Plastizitätsbedingung Für Einkristalle," J. Appl. Math. Mech., **9**(1), pp. 49–58.
[91] Voigt, W., 1928, *Lehrbuch Der Kristallphysik*, Teubner, Leipzig, Germany.
[92] Alam, M. M., Fabricius, I. L., and Christensen, H. F., 2012, "Static and Dynamic Effective Stress Coefficient of Chalk," Geophysics, **77**(2), pp. L1–L11.
[93] Fortin, J., and Guéguen, Y., 2021, "Porous and Cracked Rocks Elasticity: Macroscopic Poroelasticity and Effective Media Theory," Math. Mech. Solids, **26**(8), pp. 1158–1172.
[94] Borgomano, J. V. M., Pimienta, L., Fortin, J., and Guéguen, Y., 2017, "Dispersion and Attenuation Measurements of the Elastic Moduli of a Dual-Porosity Limestone," J. Geophys. Res. Solid Earth, **122**(4), pp. 2690–2711.
[95] Borgomano, J. V., Pimienta, L. X., Fortin, J., and Guéguen, Y., 2019, "Seismic Dispersion and Attenuation in Fluid-Saturated Carbonate Rocks: Effect of Microstructure and Pressure," J. Geophys. Res. Solid Earth, **124**(12), pp. 12498–12522.
[96] Borgomano, J. V., Gallagher, A., Sun, C., and Fortin, J., 2020, "An Apparatus to Measure Elastic Dispersion and Attenuation Using Hydrostatic-and Axial-Stress Oscillations Under Undrained Conditions," Rev. Sci. Instrum,., **91**(3), p. 034502.
[97] Yin, H., Borgomano, J. V., Wang, S., Tiennot, M., Fortin, J., and Guéguen, Y., 2019, "Fluid Substitution and Shear Weakening in Clay-Bearing Sandstone at Seismic Frequencies," J. Geophys. Res. Solid Earth, **124**(2), pp. 1254–1272.
[98] Pimienta, L., Fortin, J., and Guéguen, Y., 2015, "Bulk Modulus Dispersion and Attenuation in Sandstones," Geophysics, **80**(2), pp. D111–D127.
[99] Bishop, A. W., 1976, "The Influence of System Compressibility on the Observed Pore-Pressure Response to an Undrained Change in Stress in Saturated Rock," Geotechnique, **26**(2), pp. 371–375.
[100] Ghabezloo, S., and Sulem, J., 2010, "Effect of the Volume of the Drainage System on the Measurement of Undrained Thermo-Poro-Elastic Parameters," Int. J. Rock Mech. Min. Sci., **47**(1), pp. 60–68.
[101] Wissa, A. E., 1969, "Pore Pressure Measurements in Saturated Stiff Soils," J. Soil Mech. Found. Div., Am. Soc. Civ. Eng., **95**(4), pp. 1063–1073.
[102] Al-Wardy, W., 2003, "Analytical and Experimental Study of the Poroelastic Behaviour of Clean and Clay-Rich Sandstones," Ph.D. thesis, Imperial College London, London, UK.
[103] Green, D. H., and Wang, H. F., 1986, "Fluid Pressure Response to Undrained Compression in Saturated Sedimentary Rock," Geophysics, **51**(4), pp. 948–956.
[104] Paterson, M. S., and Wong, T. F., 2005, *Experimental Rock Deformation-The Brittle Field*, Springer Science and Business Media, Berlin.
[105] Song, I., and Renner, J., 2008, "Hydromechanical Properties of Fontainebleau Sandstone: Experimental Determination and Micromechanical Modeling," J. Geophys. Res. Solid Earth, **113**(B9), epub.
[106] Zimmerman, R. W., Somerton, W. H., and King, M. S., 1986, "Compressibility of Porous Rocks," J. Geophys. Res. Solid Earth, **91**(B12), pp. 12765–12777.
[107] Zimmerman, R. W., 2000, "Coupling in Poroelasticity and Thermoelasticity," Int. J. Rock Mech. Min. Sci,., **37**(1–2), pp. 79–87.
[108] Dassanayake, A. B., Fujii, Y., Fukuda, D., and Kodama, J. I., 2015, "A New Approach to Evaluate Effective Stress Coefficient for Strength in Kimachi Sandstone," J. Pet. Sci. Eng., **131**, pp. 70–79.
[109] Baud, P., Reuschlé, T., Ji, Y., Cheung, C. S., and Wong, T. F., 2015, "Mechanical Compaction and Strain Localization in Bleurswiller Sandstone," J. Geophys. Res. Solid Earth, **120**(9), pp. 6501–6522.
[110] van Oort, E., 1994, "A Novel Technique for the Investigation of Drilling Fluid Induced Borehole Instability in Shales," Proceedings of Rock Mechanics in Petroleum Engineering, Delft, The Netherlands, Aug. 29–31, Paper No. SPE-28064-MS.
[111] Cui, Q., 2016, "Stress Dependent Compaction in Tight Reservoirs and its Impact on Long-Term Production," Ph.D. thesis, Colorado School of Mines, Golden, CO.
[112] Bernabe, Y., 1985, "Permeability and Pore Structure of Rocks Under Pressure, Ph.D. thesis, Massachusetts Institute of Technology, Cambridge, MA.
[113] Bernabe, Y., 1986, "The Effective Pressure Law for Permeability in Chelmsford Granite and Barre Granite," Int. J. Rock Mech. Min. Sci. Geomech. Abstr., **23**(3), pp. 267–275.
[114] Teufel, L. W., and Warpinski, N. R., 1990, "Laboratory Determination of Effective Stress Laws for Deformation and Permeability of Chalk," Sandia National Labs, Albuquerque, NM, Report No. SAND-90-1113C; CONF-9006181-1.
[115] Wang, Y., Meng, F., Wang, X., Baud, P., and Wong, T. F., 2018, "Effective Stress Law for the Permeability and Deformation of Four Porous Limestones," J. Geophys. Res. Solid Earth, **123**(6), pp. 4707–4729.
[116] Meng, F., Baud, P., Ge, H., and Wong, T. F., 2019, "The Effect of Stress on Limestone Permeability and Effective Stress Behavior of Damaged Samples," J. Geophys. Res. Solid Earth, **124**(1), pp. 376–399.
[117] Chen, Z., Zheng, L., Li, M., Xiao, W., and Liu, Z., 2008, "The Effective Pressure Law for Permeability in Northern Hubei Low Permeability Sandstone Rock," Proceedings of 14th World Conference on Earthquake Engineering, China, Beijing, Oct. 12–17, pp. 12–17.
[118] Morrow, C. A., Zhang, B. C., and Byerlee, J. D., 1986, "Effective Pressure Law for Permeability of Westerly Granite Under Cyclic Loading," J. Geophys. Res. Solid Earth, **91**(B3), pp. 3870–3876.
[119] Box, G. P., and Draper, N. R., 1987, *Empirical Model-Building and Response Surfaces*, Wiley, New York.
[120] Li, M., Bernabé, Y., Xiao, W. I., Chen, Z. Y., and Liu, Z. Q., 2009, "Effective Pressure Law for Permeability of E-Bei Sandstones," J. Geophys. Res. Solid Earth, **114**(B7), epub.
[121] Warpinski, N. R., and Teufel, L. W., 1994, "Effective-Stress-Law Behavior of Austin Chalk Rocks for Deformation and Fracture Conductivity," Sandia National Labs, Albuquerque, NM, Report No. SAND-94-0012.
[122] Ma, X., and Zoback, M. D., 2017, "Laboratory Experiments Simulating Poroelastic Stress Changes Associated With Depletion and Injection in Low-Porosity Sedimentary Rocks," J. Geophys. Res. Solid Earth, **122**(4), pp. 2478–2503.
[123] Todd, T., and Simmons, G., 1972, "Effect of Pore Pressure on the Velocity of Compressional Waves in Low-Porosity Rocks," J. Geophys. Res., **77**(20), pp. 3731–3743.
[124] Prasad, M., and Manghnani, M. H., 1997, "Effects of Pore and Differential Pressure on Compressional Wave Velocity and Quality Factor in Berea and Michigan Sandstones," Geophysics, **62**(4), pp. 1163–1176.
[125] Mulchandani, V., and Sharma, R., 2017, "Sensitivity of Effective Pressure Towards V_p and V_s Using Biot's and Effective Stress Coefficients in Carbonate Reservoirs," Proceedings of International Conference on Engineering Geophysics, Society of Exploration Geophysicists, United Arab Emirates, Oct. 9–12, pp. 344–347.
[126] Sharma, R., 2015, "Impact of Texture Heterogeneity on Elastic and Viscoelastic Properties of Carbonates," Ph.D. thesis, Colorado School of Mines, Golden, CO.
[127] Salemi, H., Nourifard, N., Iglauer, S., Rezagholilou, A., and Sarmadivaleh, M., 2019, "Acoustic Approach to Determine Biot Effective Stress Coefficient of Sandstone Using True Triaxial Cell (TTSC)," Proceedings of 13th Australia and New Zealand Conference on Geomechanics, Acosta-Martinez, L., eds., Sydney, Australia, June 28–July 1, Paper No. ARMA-2020-1048.
[128] Mavko, G., and Vanorio, T., 2010, "The Influence of Pore Fluids and Frequency on Apparent Effective Stress Behavior of Seismic Velocities," Geophysics, **75**(1), pp. N1–N7.
[129] Vasquez, G. F., Vargas Junior, E. D., Ribeiro, C. J., Leão, M., and Justen, J. C., 2009, "Experimental Determination of the Effective Pressure Coefficients for Brazilian Limestones and Sandstones," Rev. Bras. Geofis., **27**(1), pp. 43–53.
[130] Xu, X., Hofmann, R., Batzle, M., and Tshering, T., 2006, "Influence of Pore Pressure on Velocity in Low-Porosity Sandstone: Implications for Time-Lapse Feasibility and Pore-Pressure Study," Geophys. Prospect., **54**(5), pp. 565–573.
[131] Christensen, N. I., and Wang, H. F., 1985, "The Influence of Pore Pressure and Confining Pressure on Dynamic Elastic Properties of Berea Sandstone," Geophysics, **50**(2), pp. 207–213.
[132] Christensen, N. I., 1984, "Pore Pressure and Oceanic Crustal Seismic Structure," Geophys. J. Int., **79**(2), pp. 411–423.
[133] Geertsma, J., 1957, "The Effect of Fluid Pressure Decline on Volumetric Changes of Porous Rocks," Pet. Trans., AIME, **210**(01), pp. 331–340.
[134] Wu, B., 2001, "Biot's Effective Stress Coefficient Evaluation: Static and Dynamic Approaches," Proc. ISRM International Symposium-Second Asian Rock Mechanics Symposium, International Society for Rock Mechanics and Rock Engineering, Beijing, China, Sept. 11–14, Paper No. ISRM-ARMS2-2001-082.
[135] Cosenza, P., Ghoreychi, M., De Marsily, G., Vasseur, G., and Violette, S., 2002, "Theoretical Prediction of Poroelastic Properties of Argillaceous Rocks From In Situ Specific Storage Coefficient," Water Resour. Res., **38**(10), p. 25.
[136] Walsh, J. B., 1965, "The Effect of Cracks on the Compressibility of Rock," J. Geophys. Res., **70**(2), pp. 381–389.
[137] Walsh, J. B., and Grosenbaugh, M. A., 1979, "A New Model for Analyzing the Effect of Fractures on Compressibility," J. Geophys. Res. Solid Earth, **84**(B7), pp. 3532–3536.

[138] Kachanov, M., 1993, "Elastic Solids With Many Cracks and Related Problems," Adv. Appl. Mech., **30**, pp. 259–445.
[139] David, E. C., and Zimmerman, R. W., 2011, "Elastic Moduli of Solids Containing Spheroidal Pores," Int. J. Eng. Sci., **49**(7), pp. 544–560.
[140] Selvadurai, A. P. S., and Suvorov, A. P., 2020, "The Influence of the Pore Shape on the Bulk Modulus and the Biot Coefficient of Fluid-Saturated Porous Rocks," Sci. Rep., **10**(1), pp. 1–10.
[141] Li, Q., Aguilera, R., and Cinco-Ley, H., 2020, "A Correlation for Estimating the Biot Coefficient," SPE Drill. Compl., **35**(02), pp. 151–163.
[142] Tan, X., and Konietzky, H., 2014, "Numerical Study of Variation in Biot Coefficient With Respect to Microstructure of Rocks," Tectonophysics, **610**, pp. 159–171.
[143] Tan, X., Konietzky, H., and Frühwirt, T., 2015, "Experimental and Numerical Study on Evolution of Biot's Coefficient During Failure Process for Brittle Rocks," Rock Mech. Rock Eng., **48**(3), pp. 1289–1296.
[144] Chen, S., Zhao, Z., Chen, Y., and Yang, Q., 2020, "On the Effective Stress Coefficient of Saturated Fractured Rocks," Comput Geotech., **123**, p. 103564.
[145] Zhao, Z., Chen, S., Chen, Y., and Yang, Q., 2021, "On the Effective Stress Coefficient of Single Rough Rock Fractures," Int. J. Rock Mech. Min. Sci., **137**, p. 104556.
[146] Coyner, K. B., 1984, "Effects of Stress, Pore Pressure, and Pore Fluids on Bulk Strain, Velocity, and Permeability in Rocks," Ph.D. thesis, Massachusetts Institute of Technology, Cambridge, MA.
[147] Hart, D. J., and Wang, H. F., 1995, "Laboratory Measurements of a Complete Set of Poroelastic Moduli for Berea Sandstone and Indiana Limestone," J. Geophys. Res. Solid Earth, **100**(B9), pp. 17741–17751.
[148] Hasanov, A. K., Prasad, M., and Batzle, M. L., 2017, "Simultaneous Measurements of Transport and Poroelastic Properties of Rocks," Rev. Sci. Instrum., **88**(12), p. 124503.
[149] Biot, M. A., 1955, "Theory of Elasticity and Consolidation for a Porous Anisotropic Solid," J. Appl. Phys., **26**(2), pp. 182–185.
[150] Carroll, M. M., 1979, "An Effective Stress Law for Anisotropic Elastic Deformation," J. Geophys. Res. Solid Earth, **84**(B13), pp. 7510–7512.
[151] Cheng, A. D., 1997, "Material Coefficients of Anisotropic Poroelasticity," Int. J. Rock Mech. Min. Sci., **34**(2), pp. 199–205.
[152] Katsube, N., 1985, "The Constitutive Theory for Fluid-Filled Porous Materials," ASME J. Appl. Mech., **52**(1), pp. 185–189.
[153] Lehner, F. K., 2011, "The Linear Theory of Anisotropic Poroelastic Solids," *Mechanics of Crustal Rocks - CISM Courses and Lectures*, Leroy, Y. M., and Lehner, F. K., eds., Springer, Wien New York, pp. 1–41.
[154] Saurabh, S., and Harpalani, S., 2018, "The Effective Stress Law for Stress-Sensitive Transversely Isotropic Rocks," Int. J. Rock Mech. Min. Sci., **101**, pp. 69–77.
[155] Thompson, M., and Willis, J. R., 1991, "A Reformation of the Equations of Anisotropic Poroelasticity," ASME J. Appl. Mech., **58**(3), pp. 612–616.
[156] Zhou, X., and Ghassemi, A., 2019, "Biot's Effective Stress Coefficient Tensor Measurements on Mancos Shale," Proceedings of 53rd U.S. Rock Mechanics/Geomechanics Symposium, American Rock Mechanics Association, ARMA, New York, June 23–26, pp. 2019–0516.
[157] Zhou, X., Ghassemi, A., Riley, S., and Roberts, J., 2017, "Biot's Effective Stress Coefficient of Mudstone Source Rocks," Proceedings of 51st U.S. Rock Mechanics/Geomechanics Symposium, American Rock Mechanics Association, San Francisco, CA, June 25–28, Report No. ARMA-2017-0235.
[158] Hassanzadegan, A., Guérizec, R., Reinsch, T., Blöcher, G., Zimmermann, G., and Milsch, H., 2016, "Static and Dynamic Moduli of Malm Carbonate: A Poroelastic Correlation," Pure Appl. Geophys., **173**(8), pp. 2841–2855.
[159] Akbarzadeh, H., and Chalaturnyk, R. J., 2014, "Structural Changes in Coal at Elevated Temperature Pertinent to Underground Coal Gasification: A Review," Int. J. Coal Geol., **131**, pp. 126–146.
[160] Klinkenberg, L. J., 1941, "The Permeability of Porous Media to Liquids and Gases," *Proceedings of Drilling and Production Practice*, American Petroleum Institute, New York, pp. 41–200.
[161] Fang, Y., Shi, Y., Sheng, Y., and Zhang, Z., 2018, "Modeling of Biot's Coefficient for a Clay-Bearing Sandstone Reservoir," Arab. J. Geosci., **11**(12), pp. 1–17.
[162] Gokaraju, D., Aldin, M., Thombare, A., Mitra, A., Govindarajan, S., and Patterson, R., 2018, "A Novel Method for Experimental Characterization of the Poroelastic Constants in Unconventional Formations," Proceedings of Unconventional Resources Technology Conference, Society of Exploration Geophysicists, American Association of Petroleum Geologists, Society of Petroleum Engineers, Houston, TX, July 23–25, pp. 3038–3051.
[163] ASTM International, 2013, "Standard Practice for Using Significant Digits in Geotechnical Data," ASTM International, West Conshohocken, PA, Paper No. ASTM D6026-13.